

# Mathematical Modeling of Stellar Evolution: A Scientific Analysis of the Life and Death of Stars

1<sup>st</sup> Vítor Fernandes Alves

*Department of Physics*

*Minho's University*

Braga, Portugal

a103940@alunos.uminho.pt

**Abstract**—This work explores the stellar life cycle from formation to eventual collapse through the lens of mathematical modeling. Bridges physics and mathematics to interpret the mechanisms that govern the evolution of stars. From interstellar clouds to the creation of black holes or white dwarfs, this study discusses the principles and equations that allow us to understand and predict stellar behavior.

**Index Terms**—Stellar Evolution, Star Life Cycle, Gravitational Collapse, Hertzsprung-Russell Diagram, Nuclear Fusion, Spectral Classification

## I. INTRODUCTION

Stars, the luminous objects scattered across the vast expanse of the cosmos, have intrigued humanity for millennia. Their radiant emissions, the result of nuclear fusion processes occurring at their cores, have not only served as navigational markers throughout history but also provided invaluable insights into the workings of the universe. These celestial bodies are fundamental components of the universe, playing a pivotal role in the formation of galaxies, the synthesis of chemical elements, and the evolution of matter. Stars are powerful sources of energy, and their life cycles dictate much of the dynamism in the cosmos. Understanding the processes by which stars form, evolve, and eventually end their existence is essential for understanding the past, present, and future of the universe.

In the context of cosmology, stars are the driving forces behind the formation and evolution of galaxies and the distribution of elements throughout the universe. Through nuclear fusion, they convert lighter elements such as hydrogen and helium into heavier elements, releasing vast amounts of energy in the process. These elements contribute to the formation of the planetary systems and, in some cases, are integral to the development of life as we know it. Consequently, the study of stellar processes is crucial not only to astronomy but also to our broader understanding of the universe. Without a comprehensive understanding of stellar physics, our grasp of the fundamental mechanisms of the universe would remain incomplete.

This work aims to bridge the disciplines of astronomy and mathematics in a detailed study of stellar evolution, the life cycle of stars, from their formation to their ultimate demise. Employing mathematical models, we will examine the physical processes involved in star formation, energy

production, and stellar death. These models, such as those describing hydrostatic equilibrium, nuclear fusion reactions, and gravitational collapse, will allow us to understand how stars evolve over time and how their life cycles influence the structure of the universe.

Mathematics is an essential tool in the study of stars. The universe is governed by physical laws, many of which can be described by mathematical equations. These equations allow scientists to predict the behavior of stars and model their evolution across various timescales, from millions to billions of years. For instance, mathematical models can predict the minimum mass required for star formation, the temperature at which nuclear fusion ignites, and the eventual fate of a star based on its mass and composition. These predictive models are crucial for understanding the processes of star formation, evolution, and death, and they enable us to forecast the future of stars and their role in the universe.

This monograph will begin by examining the intricate process of stellar formation. The birth of a star is a complex astrophysical phenomenon initiated by the gravitational collapse of interstellar gas and dust. This collapse leads to the formation of a protostar and, eventually, to the ignition of nuclear fusion within its core, signifying the onset of a star's life on the main sequence. This criterion allows us to determine the specific physical conditions, such as mass, temperature, and density, under which a molecular cloud becomes unstable and begins to collapse. Additionally, we will analyze the Hertzsprung-Russell diagram, a fundamental tool in stellar astrophysics used to classify stars according to their luminosity and surface temperature, and discuss its relevance in tracing the evolutionary path of stars.

Next, we will examine the main sequence of a star life, during which it maintains a balance between gravitational contraction and the outward pressure generated by nuclear fusion in its core. This balance, known as hydrostatic equilibrium, is vital to the stability of a star. The processes of energy transport, both through radiation and convection, will also be discussed, as they are essential for maintaining the energy balance of a star throughout its lifetime. Additionally, we will explore spectral classification, a system that categorizes stars based on their temperature and the characteristics of their spectral lines, which provides valuable insights into their physical properties.

In the later stages of stellar evolution, stars undergo dramatic

transformations, and their fates diverge depending on their mass. Low-mass stars, like our Sun, shed their outer layers and become white dwarfs, while more massive stars end their lives in supernovae, leaving behind neutron stars or, in the case of extremely massive progenitors, black holes. The mathematical models describing these processes, including the Chandrasekhar limit and the equations governing the collapse of stellar cores, will be explored in detail. We will also explore how these final stages are linked to high-energy astrophysical phenomena, including gravitational waves and pulsars.

Finally, this work will reflect on the central role of mathematics in modeling stellar behavior. The mathematical descriptions of physical laws enable us to predict the future of stars, their life cycles, and their impact on the universe. By understanding the mathematical underpinnings of stellar evolution, we gain insight not only into the stars themselves but also into the fundamental nature of the cosmos. This interdisciplinary approach highlights the importance of combining mathematics with astronomy and cosmology and suggests that future astrophysical research will continue to rely on the development of advanced mathematical models and computational simulations.

Through this exploration of stellar evolution, we will uncover how studying stars enables us to understand the broader mechanisms that shape the cosmos. Mathematical modeling of stellar processes equips us with the tools to decode the physical laws that govern the universe, linking the birth, life, and death of stars to the grand narrative of cosmic evolution.

## II. STAR FORMATION

### A. Molecular clouds and protostars

Stars are born in vast, cold regions of space known as molecular clouds, also known as stellar nurseries. These clouds are primarily made up of molecular hydrogen ( $H_2$ ), along with helium, trace molecules such as CO, and microscopic solid particles known as interstellar dust. Although they account for less than 1% of the interstellar medium (ISM) by volume, molecular clouds represent a significant fraction of its total mass. They typically span between 10 and 100 parsecs, with densities ranging from  $10^2$  to  $10^6$  particles per cubic centimeter, which is orders of magnitude higher than the average ISM density. The temperatures within these clouds are remarkably low, usually between 10 K and 20 K, making them some of the coldest environments in the universe [5].

Although they are cold, molecular clouds can be extraordinarily massive, often containing sufficient material to give rise to hundreds or even thousands of stars. When localized regions within the cloud reach a critical density, the internal thermal pressure becomes insufficient to counteract gravitational attraction, triggering gravitational collapse. This instability is governed by parameters such as the cloud's mass, temperature, and density, which will be quantitatively analyzed using the Jeans criterion, as discussed in Section II-C.

As gravitational collapse proceeds, the cloud fragments into smaller clumps, each of which can give rise to a protostar. At the center of each clump, a dense core forms and begins to

accrete mass from the surrounding material via a circumstellar disk. This marks the onset of the protostellar phase, a dynamic period characterized by increasing central temperature and pressure. During this phase, gravitational energy is converted into thermal radiation, which is the primary energy source, as nuclear fusion has not yet begun [6].

The early protostar often exhibits bipolar outflows and jets aligned with its rotational axis, driven by complex interactions between magnetic fields and accretion dynamics. These phenomena play a crucial role in regulating angular momentum and shaping the final mass of the forming star. An illustration of this process is shown in “Fig. 1”, which depicts an artist’s impression of a protostar surrounded by an accretion disk and emitting bipolar jets. These disks are believed to be the birthplaces of planetary systems such as our own solar system.

This formative stage sets the foundation for the future evolution of the stars. Once the temperature in the core reaches approximately 10 million Kelvin, hydrogen fusion begins via the proton-proton chain reaction or the CNO cycle, depending on the star’s mass. This ignition marks the transition to the main sequence phase, where the star achieves hydrostatic equilibrium and begins a stable period of nuclear burning, as discussed in Section II-D.

### B. Interstellar Extinction and the Composition of the interstellar medium

The interstellar medium (ISM) plays a fundamental role in the process of star formation, acting as both the cradle and the fuel source for stellar birth. It consists of approximately 99% gas, primarily hydrogen (both atomic and molecular) and helium, and 1% dust by mass. Despite their small mass fraction, interstellar dust grains have a disproportionate influence on the optical properties of the ISM. These dust particles absorb and



Fig. 1. Artistic rendering of the protostar L1527 showing a thick accretion disk and bipolar jets carving cavities in the surrounding gas. This image, captured by the James Webb Space Telescope’s MIRI instrument, offers insight into the early stages of star formation [1].

scatter starlight. This leads to two key phenomena: interstellar extinction (the dimming of starlight) and reddening (a shift in color due to preferential scattering of shorter wavelengths). As a result, stars seen through dusty regions appear both dimmer and redder than they truly are [5].

Extinction is wavelength dependent and is often characterized by an extinction curve, which quantifies the amount of dimming in magnitudes as a function of wavelength. Shorter wavelengths, like ultraviolet and blue light are scattered and absorbed more efficiently than longer wavelengths, like red and infrared. This wavelength dependence makes infrared astronomy particularly powerful for observing regions that are heavily obscured in visible light, such as stellar nurseries embedded within dense molecular clouds [4].

A vivid illustration of this effect can be seen in “Fig. 2”, which shows the Orion Nebula as observed in the infrared by the Spitzer Space Telescope. In this image, many young stars, completely hidden in optical wavelengths, become visible thanks to the dust penetrating power of infrared light. Such observations are crucial for unveiling the star formation occurring deep inside molecular clouds.

Observationally, key spectroscopic features help identify the dust composition. For example:

- Silicate grains produce strong absorption bands at  $9.7\text{ }\mu\text{m}$  and  $18\text{ }\mu\text{m}$ .
- Graphite and PAHs exhibit a broad absorption feature around  $217.5\text{ nm}$ .
- Ices, when present in cold molecular clouds, show additional features in the  $3\text{ }\mu\text{m}$  region.

The gas component of the ISM is equally critical and can be studied through emission lines. One of the most important is the  $21\text{ cm}$  line of neutral hydrogen ( $\text{H I}$ ), which arises from the hyperfine transition and allows astronomers to map the structure, dynamics, and distribution of hydrogen gas across galaxies [5].

### C. Gravitational Collapse: Jeans criterion and Free-Fall time scale

Gravitational collapse is the fundamental process by which dense regions within molecular clouds overcome internal pressure and begin to contract, eventually leading to the formation of stars. In this section, we derive two key concepts. First, the Jeans criterion, which specifies the conditions under which a perturbation in a gas cloud becomes unstable and collapses under its own gravity; and second, the free-fall timescale, which gives an estimate of the time it takes for a cloud to collapse to form a protostar. These derivations are critical for understanding the early stages of star formation.

#### Deriving the Jeans Mass

We begin with a uniform spherical gas cloud of radius  $R$ , mass  $M$ , density  $\rho_0$ , and temperature  $T$ . We apply the virial theorem and analyze gravitational and thermal energy.

To compute the total gravitational potential energy  $U$  of a solid sphere of mass  $M$  and radius  $R$ , we consider the process of assembling the sphere shell by shell under the influence

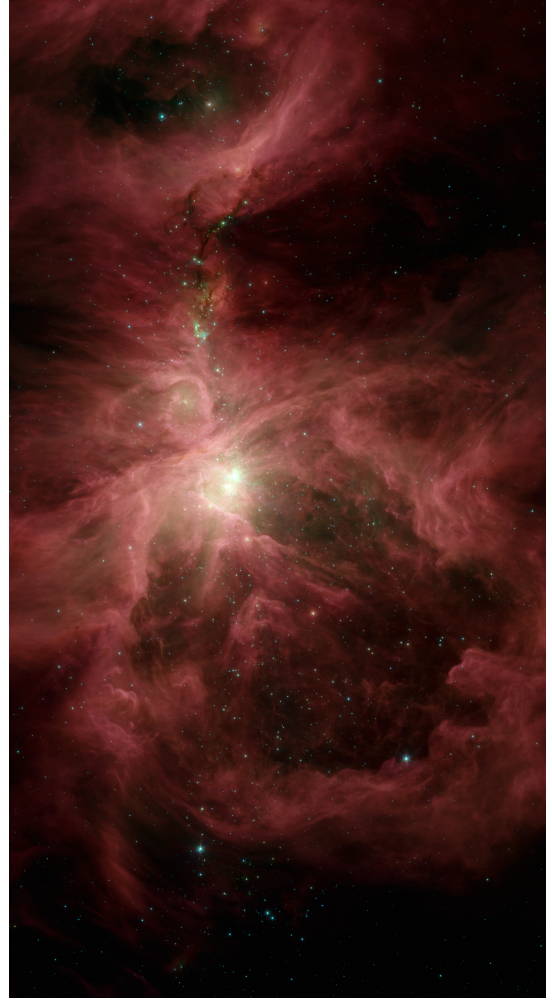


Fig. 2. Infrared image of the Orion Nebula from NASA’s Spitzer Space Telescope. This image highlights the star-forming regions obscured by interstellar dust, which is typically invisible in optical wavelengths. Infrared observations are crucial for studying star formation in such dusty regions [2].

of gravity. At each stage, a spherical shell of radius  $r$  and infinitesimal thickness  $dr$  is added to a sphere of mass  $M(r)$ , representing the mass already assembled up to that radius.

The differential gravitational energy required to bring this shell from infinity to radius  $r$  is given by:

$$dU = -\frac{GM(r)dm}{r}, \quad (1)$$

where  $G$  is the gravitational constant,  $M(r)$  is the mass inside the radius  $r$ , and  $dm$  is the mass of the added shell.

Assuming that the sphere has a uniform density  $\rho_0$ , we have:

$$\rho_0 = \frac{M}{\frac{4}{3}\pi R^3}. \quad (2)$$

The mass within radius  $r$  is:

$$M(r) = \rho_0 \cdot \frac{4}{3}\pi r^3, \quad (3)$$

and the mass of the shell is:

$$dm = \rho_0 \cdot dV = \rho_0 \cdot 4\pi r^2 dr. \quad (4)$$

Substituting into the expression for  $dU$ , we obtain:

$$dU = -\frac{G \cdot \left(\frac{4}{3}\pi r^3 \rho_0\right) \cdot (4\pi r^2 \rho_0 dr)}{r} = -\frac{16}{3}\pi^2 G \rho_0^2 r^4 dr. \quad (5)$$

Integrating this expression from  $r = 0$  to  $r = R$  gives the total gravitational potential energy:

$$U = \int_0^R dU = -\frac{16}{3}\pi^2 G \rho_0^2 \int_0^R r^4 dr = -\frac{16}{15}\pi^2 G \rho_0^2 R^5. \quad (6)$$

Changing  $\rho$  by its expression in terms of  $M$  and  $R$ , we find:

$$\rho_0 = \frac{3M}{4\pi R^3} \Rightarrow \rho_0^2 = \frac{9M^2}{16\pi^2 R^6}. \quad (7)$$

Substituting into the expression for  $U$ :

$$U = -\frac{16}{15}\pi^2 G \cdot \frac{9M^2}{16\pi^2 R^6} \cdot R^5 = -\frac{9}{15}\frac{GM^2}{R} = -\frac{3}{5}\frac{GM^2}{R}. \quad (8)$$

Hence, the gravitational binding energy of a homogeneous solid sphere is

$$U = -\frac{3}{5}\frac{GM^2}{R} \quad (9)$$

The internal thermal energy  $K$  of an ideal gas is directly related to its temperature and the number of particles. For a monatomic ideal gas, the total internal energy is given by:

$$K = \frac{3}{2}NkT, \quad (10)$$

where  $N$  is the number of particles,  $k$  is the Boltzmann constant, and  $T$  is the temperature in Kelvin.

To express this in terms of the gas mass  $M$ , we note that the number of particles can be written as:

$$N = \frac{M}{\mu m_H}, \quad (11)$$

where  $\mu$  is the mean molecular weight and  $m_H$  is the mass of a hydrogen atom. Substituting this into the expression for  $K$ , we get:

$$K = \frac{3}{2} \cdot \frac{M}{\mu m_H} \cdot kT. \quad (12)$$

Therefore, the internal energy of a monatomic ideal gas becomes the following.

$$K = \frac{3}{2} \frac{MkT}{\mu m_H}. \quad (13)$$

Using the Virial Theorem, which describes the equilibrium situation as  $2K + U = 0$ , and Eqs. 9 and 13, we obtain the following.

$$2K + U = 2 \cdot \frac{3}{2} \frac{MkT}{\mu m_H} - \frac{3}{5} \frac{GM^2}{R} = 0. \quad (14)$$

Now, isolating  $M$ , we obtain

$$M = \frac{5kTR}{G\mu m_H}. \quad (15)$$

Now express  $R$  in terms of the density  $\rho_0$ , we have

$$R = \left( \frac{3M}{4\pi\rho_0} \right)^{1/3} \quad (16)$$

Now, substitute this expression for  $R$  in Eq. 15:

$$M = \frac{5kT}{G\mu m_H} \left( \frac{3M}{4\pi\rho_0} \right)^{1/3} \quad (17)$$

Taking the power of 3 on both sides, canceling  $M$  from both sides, and after taking the square root of both sides, we obtain

$$M = \sqrt{\left( \frac{5kT}{G\mu m_H} \right)^3 \cdot \frac{3}{4\pi\rho_0}} \quad (18)$$

Thus, we find that the Jeans mass  $M_J$  is [5], [6]

$$M_J \equiv M \approx \left( \frac{G\mu m_H}{5kT} \right)^{3/2} \left( \frac{4\pi\rho_0}{3} \right)^{1/2} \quad (19)$$

This result shows that a gas cloud will collapse gravitationally when its mass exceeds  $M_J$ .

#### Free-Fall Timescale Derivation

Once a region becomes gravitationally unstable, when its mass exceeds the Jeans mass, it will begin to collapse. The free fall timescale is an estimate of how quickly a cloud will collapse under gravity in the absence of any opposing pressure.

Using the conservation of energy for a particle: initially, the particle has potential energy and is at rest, and at any point during the fall, we obtain the following result.

$$\frac{1}{2} dm \dot{r}^2 - \frac{GM(r) dm}{r} = -\frac{GM(r_0) dm}{r_0} \quad (20)$$

where  $r_0$  is the initial radius of the cloud. Now, using Eq. 3, we obtain

$$\frac{1}{2} \dot{r}^2 - \frac{3}{4}\pi G \rho r^2 = -\frac{3}{4}\pi G \rho r_0^2 \quad (21)$$

Isolating  $\dot{r}$ , we obtain the following result.

$$\dot{r} = -\sqrt{\frac{3}{2}\pi G \rho (r_0^2 - r^2)} \quad (22)$$

The minus sign reflects that the radius is decreasing over time during collapse.

Now we separate the variables to integrate and find the fall time  $t_D$ :

$$dt = \frac{dr}{\dot{r}} = -\frac{dr}{\sqrt{\frac{3}{2}\pi G\rho(r_0^2 - r^2)}} \quad (23)$$

We make the substitution:

$$r = r_0 \cos \theta \Rightarrow dr = -r_0 \sin \theta d\theta \quad (24)$$

Substituting into the integral:

$$dt = \frac{r_0 \sin \theta d\theta}{\sqrt{\frac{3}{2}\pi G\rho(r_0^2 - r_0^2 \cos^2 \theta)}} = \frac{r_0 \sin \theta d\theta}{\sqrt{\frac{3}{2}\pi G\rho r_0^2 \sin^2 \theta}} \quad (25)$$

We can cancel  $\sin \theta$  and factor out  $r_0$ :

$$dt = \frac{r_0 d\theta}{\sqrt{\frac{3}{2}\pi G\rho r_0^2}} = \frac{d\theta}{\sqrt{\frac{3}{2}\pi G\rho}} \quad (26)$$

Now integrate from  $\theta = 0$  to  $\theta = \frac{\pi}{2}$ :

$$t_D = \int_0^{\pi/2} dt = \int_0^{\pi/2} \frac{d\theta}{\sqrt{\frac{3}{2}\pi G\rho}} = \frac{\pi}{2} \cdot \frac{1}{\sqrt{\frac{3}{2}\pi G\rho}} \quad (27)$$

Thus, the final result for the free-fall time is as follows:

$$t_D = \sqrt{\frac{3\pi}{32G\rho}} \quad (28)$$

This timescale gives an order of magnitude estimate of the time it takes for the entire cloud to collapse under its own gravity if no pressure or other forces counteract the collapse.

The free fall time represents a lower limit for the collapse phase. In reality, the collapse of a cloud into a protostar involves slower processes, such as energy loss through radiation (Kelvin-Helmholtz contraction), before the core temperature reaches the levels required for sustained nuclear fusion. For many stars, especially those with a mass similar to the Sun, the time from the onset of collapse to the ignition of hydrogen fusion, the arrival on the main sequence, spans millions of years. However, the free-fall time scale serves as a fundamental dynamical limit for the collapse process.

#### D. Hertzsprung-Russell Diagram and the Arrival at the Main Sequence

After the protostellar phase, once the central temperature of a collapsing gas core reaches approximately 10 million Kelvin, the nuclear fusion of hydrogen into helium ignites in the core. This marks the true birth of a star and its transition into the main sequence, a stable phase during which the star achieves hydrostatic equilibrium, balancing gravitational collapse with pressure from fusion-generated radiation.

Importantly, the time it takes for a protostar to reach the main sequence is approximately given by the free-fall timescale, Eq. 28. However, the actual time to reach the main sequence is longer due to the effects of accretion, radiative losses, convection, and magnetic fields, and is more accurately represented by the Kelvin-Helmholtz timescale, which can

extend up to 10 million years for solar mass stars [5] [6]. This duration decreases with increasing stellar mass, as higher mass leads to faster core heating and earlier ignition of fusion.

Thus, a star's arrival at the main sequence is not instantaneous but is the result of a dynamic and prolonged collapse governed by physical parameters, a fact that adds further meaning to its final resting place on the H-R diagram. From there, the star begins the longest and most stable period of its life, burning hydrogen and gradually evolving in luminosity and temperature.

At this point, the star settles at a particular location on the Hertzsprung–Russell (H-R) diagram, a powerful tool used to classify stars and understand their evolution. The diagram plots stellar luminosity (vertical axis) against surface temperature (or spectral class, horizontal axis, decreasing left to right). Most stars lie along the main sequence, a band that stretches from hot, massive O- and B-type stars in the upper left to cool, low-mass M-type red dwarfs in the lower right, as shown in “Fig. 3”.

In “Fig. 3” it can be seen that the position of a star on the H-R diagram is determined primarily by its mass, which dictates its core pressure and temperature, and thus its luminosity and effective surface temperature. A more massive star has greater gravitational compression, leading to a hotter core, more rapid fusion, and higher energy output, placing it higher and to the left of the diagram. In contrast, lower-mass stars, such as red dwarfs, are cooler and less luminous, and therefore lie at the lower right [5].

Our Sun is a typical G2V star, the spectral class G2 indicates a surface temperature of about 5778 K, while the luminosity class V designates a main-sequence star (or ‘dwarf’). The Sun has been in the main sequence for about 4.6 billion years and is expected to remain there for another 5–6 billion years before

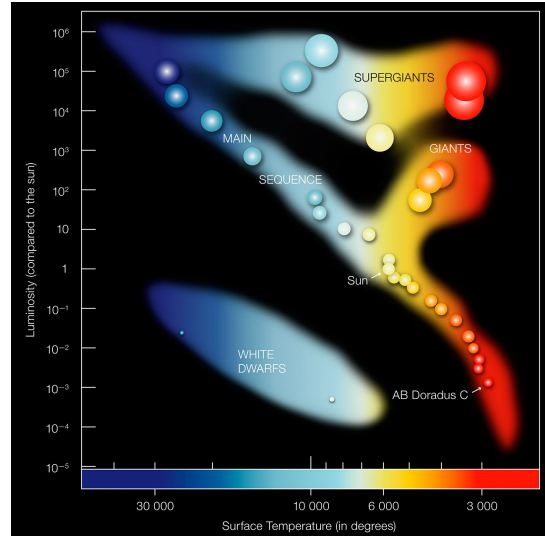


Fig. 3. The Hertzsprung–Russell Diagram. Stars on the main sequence form a diagonal band, with hot, massive stars in the upper left and cool, low-mass stars in the lower right. Giants and supergiants lie above, while white dwarfs occupy the bottom left [3].

evolving into a red giant.

Stars remain on the main sequence for most of their lifetimes, in the phase of core hydrogen burning. The duration of this stage varies drastically with mass:

- A massive O-type star may remain on the main sequence for only a few million years,
- Whereas a low-mass M-type red dwarf can persist for trillions of years, far longer than the current age of the universe.

This relationship arises because fusion rates scale steeply with mass: more massive stars burn their fuel much more quickly.

The H-R diagram is not static; stars move across it as they evolve. Once hydrogen is depleted in the core, the star leaves the main sequence and begins to traverse other regions of the diagram, expanding into a red giant or evolving toward more exotic endpoints such as white dwarfs, neutron stars, or black holes. These shifts on the diagram visually trace the changing structure of the star and energy generation mechanisms [6].

The diagram also helps reveal entire stellar populations [4] [7]:

- Open clusters, like the Pleiades, show many young stars in the main sequence.
- Globular clusters, older and metal-poor, have stars that have already evolved off the main sequence, forming a red-giant branch.

Studying the H-R diagram not only reveals the present condition of a star but also hints at its past formation and future fate. In stellar clusters, the shape of the main sequence and the turn-off point offer astronomers a way to estimate cluster ages, a technique fundamental to understanding galactic evolution.

### III. LIFE OF THE STARS

Once a star reaches the main sequence on the Hertzsprung-Russell diagram, it enters the longest and most stable phase of its life cycle. During this time, it maintains a delicate balance between gravitational collapse and outward pressure from energy generated in its core, a state governed by physical laws that can be described mathematically.

#### A. Hydrostatic Equilibrium

Hydrostatic equilibrium is the state of balance in a star between the gravitational force pulling matter inward and the thermal pressure pushing outward. This balance is crucial for maintaining the stability of the star. If disturbed, a star could collapse or expand, depending on the nature of the imbalance.

#### Deriving the Hydrostatic Equilibrium Equation

Consider a thin spherical shell inside a star, located at radius  $r$ , with infinitesimal thickness  $dr$ , density  $\rho(r)$ , and mass element  $dm$ . The mass of the shell is given by:

$$dm = \rho(r) \cdot 4\pi r^2 dr \quad (29)$$

Let  $M(r)$  be the total mass enclosed within radius  $r$ , defined by the differential relation:

$$\frac{dM}{dr} = 4\pi r^2 \rho(r), \quad (30)$$

which, upon integration from the center out to the radius  $r$ , yields:

$$M(r) = \int_0^r 4\pi r'^2 \rho(r') dr'. \quad (31)$$

Now, consider the forces acting on the shell. The gravitational force pulling the shell inward due to the enclosed mass  $M(r)$  is given by Newton's law of gravitation:

$$\begin{aligned} F_{\text{grav}} &= -\frac{GM(r)dm}{r^2} \\ &= -\frac{GM(r)\rho(r)4\pi r^2 dr}{r^2} \\ &= -4\pi GM(r)\rho(r) dr, \end{aligned} \quad (32)$$

where  $G$  is the gravitational constant. The negative sign indicates that the force is directed toward the center of the star.

Unlike this, there is an outward force due to the pressure gradient in the star. This force results from the difference in pressure between the inner and outer faces of the shell. The pressure on the inner face is  $P(r)$ , acting outward, and on the outer face is  $P(r+dr)$ , acting inward. The net pressure force on the shell is given by

$$\begin{aligned} F_{\text{pressure}} &= P(r) \cdot A - P(r+dr) \cdot A \\ &= -[P(r+dr) - P(r)] \cdot A, \end{aligned} \quad (33)$$

where  $A = 4\pi r^2$  is the area of the shell. Expanding  $P(r+dr)$  to the first order, we have the following:

$$P(r+dr) \approx P(r) + \frac{dP}{dr} dr. \quad (34)$$

So, the inward-directed force acting on the shell as a result of the pressure gradient is given by:

$$F_{\text{pressure}} = -\left(\frac{dP}{dr} dr\right) \cdot 4\pi r^2 = -\frac{dP}{dr} \cdot 4\pi r^2 dr. \quad (35)$$

In hydrostatic equilibrium, these two forces exactly cancel:

$$F_{\text{grav}} + F_{\text{pressure}} = 0 \quad (36)$$

Substituting the above expressions, Eqs. (32) and (35), we obtain:

$$-\frac{GM(r)\rho(r)}{r^2} \cdot 4\pi r^2 dr - \frac{dP}{dr} \cdot 4\pi r^2 dr = 0 \quad (37)$$

Dividing both sides by  $4\pi r^2 dr$  and simplifying:

$$\frac{dP}{dr} = -\frac{GM(r)\rho(r)}{r^2}$$

(38)

This equation describes how the internal pressure of a star must vary with radius to perfectly balance the inward pull of gravity ([5], [8]). Gravity continuously attempts to compress the stellar material toward the center, driven by the mass accumulated within a given radius  $r$ . Meanwhile, pressure, produced by the thermal motion of particles and sustained by

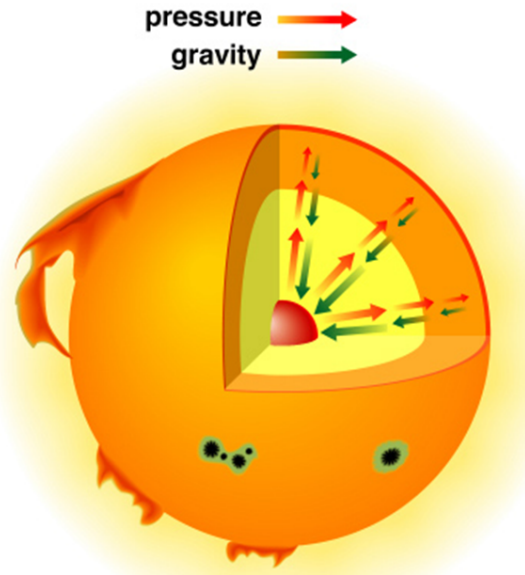


Fig. 4. Balance between gravitational pull and pressure force inside a star.

the energy released from nuclear fusion, acts outward, resisting gravitational collapse. For a star to remain stable, these two opposing forces must be exactly balanced at every point inside the star.

This delicate balance prevents the star from collapsing under its own gravity or from expanding uncontrollably due to excess internal pressure. The pressure is highest at the core, where gravity is most intense, and it gradually decreases toward the stellar surface. This gradient allows stars to maintain their structure and size for the vast majority of their lifetimes.

A helpful visual representation of this balance is provided in “Fig. 4”, where the green arrows represent gravitational force pulling inward and the red arrows indicate pressure pushing outward:

This “Fig. 4” illustrates that, at each radial shell within the star, the gravitational force is exactly countered by the pressure gradient. This hydrostatic equilibrium is critical for the stability of stars during the main phases of their evolution.

Deep inside the star, where temperatures and densities are extreme, nuclear fusion in the core produces a tremendous amount of energy. This energy increases the thermal pressure, which acts outward to support the weight of the overlying layers. The “Fig. 5” shows a full stellar cross section, highlighting the core, the pressure gradient, and how energy is transported outward.

In this structure, pressure and gravity are strongest near the core, where the density and fusion rates are highest. Farther out, both forces weaken, but the balance is preserved. This ensures that the star remains nearly spherical and structurally stable for billions of years.

If this balance were ever disrupted, if gravity momentarily overpowered pressure, or vice versa, the result would be a dramatic change: gravitational collapse, expansion, or even a

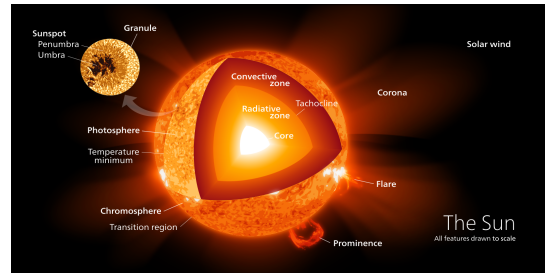


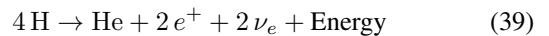
Fig. 5. Internal structure of the Sun, showing the core (fusion region), radiative and convective zones.

catastrophic explosion. Thus, this deceptively simple equation encapsulates the fragile yet stable nature of stars and is one of the most important principles in understanding stellar physics.

### B. Nuclear Fusion in Stars

The process of nuclear fusion is the primary mechanism by which a star generates energy. Fusion occurs in the core of the star, where the temperature and pressure are high enough to overcome the electrostatic repulsion between atomic nuclei. This process releases vast amounts of energy, which counteracts the inward pull of gravity, thus maintaining the star’s stability through hydrostatic equilibrium.

In the cores of stars, the temperature can exceed millions of Kelvin, providing the necessary energy to overcome the Coulomb barrier between atomic nuclei. The most common fusion process in main-sequence stars is the proton-proton chain reaction, which converts hydrogen into helium. The basic reaction can be summarized as follows.



where:

- H represents a proton (a hydrogen nucleus),
- He is the resulting helium nucleus,
- $e^+$  is the positron,
- $\nu_e$  is the electron neutrino,
- Energy is released as gamma radiation and kinetic energy of the resulting particles.

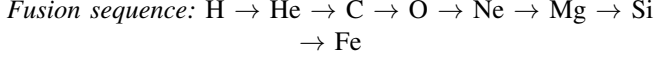
### C. Fusion Sequence in Stars

The fusion sequence within stars evolves through various stages depending on the star’s mass and age. Initially, stars fuse hydrogen into helium via the proton-proton chain or the CNO cycle. Once hydrogen in the core is depleted, fusion progresses to the formation of heavier elements:

- Helium fusion forms carbon and oxygen.
- In more massive stars, further fusion occurs producing neon, magnesium, and silicon.
- Eventually, the process leads to the production of iron.

The fusion of elements lighter than iron releases energy, but fusion of iron or heavier elements consumes energy. Once iron accumulates in the core, fusion can no longer maintain the outward pressure against gravity, and the star becomes unstable.

The ultimate fate of the star depends on its mass. For massive stars, this culminates in a supernova explosion, during which elements heavier than iron (such as gold and uranium) are synthesized via rapid neutron capture (r-process).



#### D. Energy Transport (Radiation and Convection)

In stellar interiors, energy produced through nuclear fusion in the core must be transported to the star's surface and eventually radiated into space. This energy transport primarily occurs through two physical processes: radiation and convection. The mechanism dominates and depends on local physical conditions, such as temperature, opacity, and density.

1) *Radiative Energy Transport*: Radiative transport, the process by which photons diffuse through stellar material, plays a key role in energy transfer. Due to frequent absorption, emission, and scattering interactions, photons undergo a random walk, gradually moving outward. This process depends on factors such as opacity and temperature and is governed by a temperature gradient, ensuring a net outward flow of energy, especially in radiative zones where convection is inefficient.

A crucial quantity associated with radiation is the radiation pressure, which arises because photons, although massless, carry momentum. When photons are absorbed or scattered by matter, they impart momentum and thus exert a force per unit area, a pressure. The radiation pressure is especially significant in the high-temperature interiors of massive stars.

To derive the expression for the radiation pressure, we start with the fact that each photon has energy  $E = h\nu$  and momentum  $p_\gamma = h\nu/c$ .

The pressure exerted by a gas of particles can generally be written as follows.

$$P = \frac{1}{3} \int v p f(p) dp \quad (40)$$

For photons, this becomes:

$$P_{\text{rad}} = \frac{1}{3} \int_0^\infty h\nu n(\nu) d\nu \quad (41)$$

Here,  $n(\nu) d\nu$  is the number density of photons in the frequency interval  $[\nu, \nu + d\nu]$ . The product  $h\nu \cdot n(\nu) d\nu$  represents the energy density per frequency interval,  $u_\nu d\nu$ , so we can write:

$$P_{\text{rad}} = \frac{1}{3} \int_0^\infty u_\nu d\nu = \frac{1}{3} u \quad (42)$$

The total energy density  $u$  is obtained from Planck's law for black body radiation:

$$u_\nu = \frac{8\pi h\nu^3}{c^3} \cdot \frac{1}{e^{h\nu/kT} - 1} \quad (43)$$

Integrating the Planck energy distribution over all frequencies yields the total energy density of blackbody radiation:

$$u = \int_0^\infty u_\nu d\nu = \frac{8\pi h}{c^3} \int_0^\infty \frac{\nu^3}{e^{h\nu/kT} - 1} d\nu \quad (44)$$

Using the substitution  $x = \frac{h\nu}{kT}$ , we get:

$$u = \frac{8\pi h}{c^3} \left( \frac{kT}{h} \right)^4 \int_0^\infty \frac{x^3}{e^x - 1} dx \quad (45)$$

The integral  $\int_0^\infty \frac{x^3}{e^x - 1} dx = \frac{\pi^4}{15}$  is a standard result that gives:

$$u = \frac{8\pi^5 k^4}{15 h^3 c^3} T^4 \quad (46)$$

We define the radiation constant:

$$a = \frac{8\pi^5 k^4}{15 h^3 c^3} = \frac{4\sigma}{c} \quad (47)$$

Hence, the energy density becomes  $u = aT^4$ , and the radiation pressure in a star is given by [5]:

$$P_{\text{rad}} = \frac{1}{3} a T^4 = \frac{4\sigma}{3c} T^4 \quad (48)$$

Taking the derivative with respect to radius:

$$\frac{dP_{\text{rad}}}{dr} = \frac{4\sigma}{3c} \frac{dT^4}{dr} = \frac{16\sigma T^3}{3c} \frac{dT}{dr} \quad (49)$$

2) *Radiative Transfer and the Radiation Pressure Gradient*: We consider a beam of parallel light rays of wavelength  $\lambda$  traveling through a gas. Any process that removes photons from the beam, whether it is true absorption by atomic or molecular transitions or scattering, is collectively termed *absorption*. In contrast, processes that add photons to the beam, such as atomic emission or scattering into the beam, are termed *emission*.

The infinitesimal decrease in the specific intensity  $I_\lambda$  due to absorption over a path element  $ds$  (measured along the ray) in a gas of density  $\rho$  is given by:

$$dI_\lambda = -\kappa_\lambda \rho I_\lambda ds, \quad (50)$$

where  $\kappa_\lambda$  is the *monochromatic opacity* (absorption coefficient), with units  $\text{m}^2 \text{kg}^{-1}$ , generally depending on composition,  $\rho$ , and temperature.

Similarly, the pure emission term (in the absence of absorption) takes the form:

$$dI_\lambda = j_\lambda \rho ds, \quad (51)$$

where  $j_\lambda$  is the *emission coefficient* (units  $\text{W m}^{-3} \text{sr}^{-1}$ ), which also varies with  $\lambda$ . Combining Eqs. (50) and (51) yields the full change in intensity:

$$dI_\lambda = (-\kappa_\lambda I_\lambda + j_\lambda) \rho ds. \quad (52)$$

It is customary to introduce the *source function*:  $S_\lambda \equiv j_\lambda/\kappa_\lambda$ , which has the same units as  $I_\lambda$ . Dividing Eq. (52) by  $-\kappa_\lambda \rho ds$  and defining the monochromatic optical depth

$$d\tau_\lambda = -\kappa_\lambda \rho ds, \quad (53)$$

we obtain the standard form of the radiative transfer equation:

$$\frac{dI_\lambda}{d\tau_\lambda} = I_\lambda - S_\lambda. \quad (54)$$

In a stellar atmosphere approximated as a plane-parallel slab, it is convenient to replace the physical path length  $s$  with an optical depth coordinate. The monochromatic optical depth along an arbitrary ray is defined by Eq. (53). For a ray inclined at an angle  $\theta$  with respect to the local vertical  $z$ , we define the *vertical* optical depth as:

$$\tau_{\lambda,v}(z) = \int_z^0 \kappa_\lambda \rho dz', \quad (55)$$

so that  $d\tau_{\lambda,v} = -\kappa_\lambda \rho dz$ . From the geometry illustrated in Fig. 6, we have the relation  $dz = ds \cos \theta$ , which allows us to express the total optical depth in terms of the vertical:

$$\tau_\lambda = \frac{\tau_{\lambda,v}}{\cos \theta} = \tau_{\lambda,v} \sec \theta. \quad (56)$$

Substituting Eq. (56) into Eq. (54), we obtain the standard form of the transfer equation used in a plane-parallel gray atmosphere:

$$\cos \theta \frac{dI_\lambda}{d\tau_{\lambda,v}} = I_\lambda - S_\lambda. \quad (57)$$

In the gray approximation, where the opacity is assumed to be independent of wavelength ( $\kappa_\lambda \rightarrow \kappa$ ), one may integrate over all  $\lambda$  to obtain:

$$\cos \theta \frac{dI}{d\tau_v} = I - S, \quad (58)$$

where  $\tau_v$  is the wavelength-independent vertical optical depth, and  $I, S$  are the corresponding frequency-integrated intensity and source function. This equation provides the foundation for deriving the temperature-depth relation and quantifying limb darkening in gray model atmospheres.

To derive the radiation pressure gradient in a gray plane-parallel stellar atmosphere, we begin with the same transfer equation, now emphasizing the angular dependence explicitly as  $I(\tau_v, \theta)$  and  $S(\tau_v)$ , where  $\theta$  is the angle with

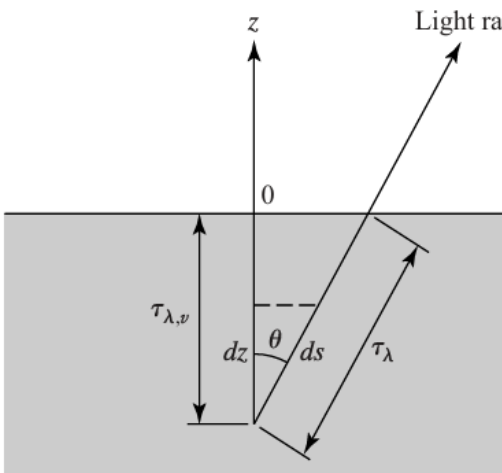


Fig. 6. Geometry of radiative transfer in a plane-parallel atmosphere. A light ray travels along a path  $ds$  at an angle  $\theta$  to the vertical axis  $z$ , passing through a corresponding optical depth  $\tau_\lambda$ . The associated vertical optical depth is denoted by  $\tau_{\lambda,v}$ .

respect to the vertical. In local thermodynamic equilibrium (LTE), the source function is equal to the mean intensity:  $S = J(\tau_v)$ .

We define the angular moments of the radiation field as:

$$J(\tau_v) = \frac{1}{2} \int_0^\pi I(\tau_v, \theta) \sin \theta d\theta, \quad (59)$$

$$F_{\text{rad}}(\tau_v) = 2\pi \int_0^\pi I(\tau_v, \theta) \cos \theta \sin \theta d\theta, \quad (60)$$

$$P_{\text{rad}}(\tau_v) = \frac{2\pi}{c} \int_0^\pi I(\tau_v, \theta) \cos^2 \theta \sin \theta d\theta. \quad (61)$$

To obtain the first moment of the transfer equation, we begin by differentiating the radiative flux  $F_{\text{rad}}(\tau_v)$ , Eq. (60) with respect to  $\tau_v$ :

$$\begin{aligned} \frac{dF_{\text{rad}}}{d\tau_v} &= \frac{d}{d\tau_v} \left[ 2\pi \int_0^\pi I(\tau_v, \theta) \cos \theta \sin \theta d\theta \right] \\ &= 2\pi \int_0^\pi \frac{dI(\tau_v, \theta)}{d\tau_v} (\tau_v, \theta) \cos \theta \sin \theta d\theta. \end{aligned} \quad (62)$$

Substituting Eq. (58) into the integrand yields the following

$$\frac{dF_{\text{rad}}}{d\tau_v} = 2\pi \int_0^\pi (I(\tau_v, \theta) - S(\tau_v)) \sin \theta d\theta. \quad (63)$$

The first term gives  $2J(\tau_v)$ , and the second is simply  $2S(\tau_v)$ , so we obtain:

$$\frac{dF_{\text{rad}}}{d\tau_v} = 4\pi (J(\tau_v) - S(\tau_v)). \quad (64)$$

In the gray LTE approximation, where  $S = J$ , this reduces to:

$$\frac{dF_{\text{rad}}}{d\tau_v} = 0 \implies F_{\text{rad}} = \text{constant}.$$

This result reflects the condition of radiative equilibrium: in an equilibrium stellar atmosphere, each process of absorption is exactly balanced by a corresponding emission process. Consequently, there is no net gain or loss of radiative energy at any point, and the radiative flux  $F_{\text{rad}}$  remains constant throughout the atmosphere.

To obtain the second moment of the transfer equation, Eq. (61), we begin by taking the derivative of the radiation pressure with respect to the vertical optical depth:

$$\begin{aligned} \frac{dP_{\text{rad}}}{d\tau_v} &= \frac{d}{d\tau_v} \left( \frac{2\pi}{c} \int_0^\pi I(\tau_v, \theta) \cos^2 \theta \sin \theta d\theta \right) \\ &= \frac{2\pi}{c} \int_0^\pi \frac{dI(\tau_v, \theta)}{d\tau_v} \cos^2 \theta \sin \theta d\theta. \end{aligned} \quad (65)$$

Now, substituting Eq. (58) into the integral:

$$\frac{dP_{\text{rad}}}{d\tau_v} = \frac{2\pi}{c} \int_0^\pi (I(\tau_v, \theta) - S) \cos \theta \sin \theta d\theta. \quad (66)$$

This expression is identical to the integrand that defines the radiative flux  $F_{\text{rad}}$ , Eq. (64), so we obtain:

$$\frac{dP_{\text{rad}}}{d\tau_v} = \frac{F_{\text{rad}}}{c}. \quad (67)$$

We can separate the integral into two terms:

$$\frac{dP_{\text{rad}}}{d\tau_v} = \frac{2\pi}{c} \left[ \int_0^\pi I(\tau_v, \theta) \cos \theta \sin \theta d\theta - S \int_0^\pi \cos \theta \sin \theta d\theta \right] \quad (68)$$

The second integral vanishes because:

$$\int_0^\pi \cos \theta \sin \theta d\theta = 0.$$

Therefore, we are left with:

$$\frac{dP_{\text{rad}}}{d\tau_v} = \frac{2\pi}{c} \int_0^\pi I(\tau_v, \theta) \cos \theta \sin \theta d\theta. \quad (69)$$

Comparing this expression with the definition of radiative flux, Eq. (60), we identify the integrand as  $F_{\text{rad}}$ , so:

$$\frac{dP_{\text{rad}}}{d\tau_v} = \frac{F_{\text{rad}}}{c}. \quad (70)$$

Using the differential relation between optical depth and geometric depth,  $d\tau_v = -\kappa\rho dr$ , we finally arrive at:

$$\frac{dP_{\text{rad}}}{dr} = -\frac{\kappa\rho}{c} F_{\text{rad}}, \quad (71)$$

which expresses the spatial gradient of radiation pressure in a gray atmosphere [5].

3) *Radiative Temperature Gradient*: Equating both expressions for  $\frac{dP_{\text{rad}}}{dr}$ , Eqs. 49 and 71:

$$\frac{16\sigma T^3}{3c} \frac{dT}{dr} = -\frac{\kappa\rho}{c} F_{\text{rad}} \quad (72)$$

Multiplying both sides by  $\frac{3c}{16\sigma T^3}$ :

$$\frac{dT}{dr} = -\frac{3\kappa\rho}{16\sigma T^3} F_{\text{rad}} \quad (73)$$

Now express the radiative flux  $F_{\text{rad}}$  in terms of local luminosity  $L(r)$ :

$$F_{\text{rad}} = \frac{L(r)}{4\pi r^2} \quad (74)$$

Substitute in the gradient expression:

$$\left. \frac{dT}{dr} \right|_{\text{rad}} = -\frac{3\kappa\rho L(r)}{64\pi\sigma r^2 T^3} \quad (75)$$

This is the radiative temperature gradient inside a star, assuming that radiative transport dominates.

This equation explains how the temperature must change with the radius for the radiation to effectively transport energy outward from the star's core. When the opacity  $\kappa$  is high because of the presence of abundant elements or dense gas, photons are more likely to be absorbed or scattered, which requires a steeper temperature gradient to drive the necessary radiative flux. Similarly, in regions of higher density or lower temperature, the gradient needs to be even steeper.

This delicate energy transfer mechanism, in which photons diffuse under the influence of a radiation pressure gradient, is crucial to the star's structure and evolution. It plays a particularly important role in the radiative zones of stars, where convection is inefficient.

4) *Convective Transport*: In stellar interiors, convection is one of the primary mechanisms for transporting energy from the core to the outer layers. It occurs when radiation becomes inefficient at carrying energy, usually due to high opacity or steep temperature gradients. In such regions, hot gas rises and cooler gas sinks, creating a convective cycle.

Consider a convective bubble that rises adiabatically in a star. As it rises, it expands and cools. From the differential form of the ideal gas law:

$$\frac{dP}{dr} = \frac{P}{\mu} \frac{d\mu}{dr} + \frac{P}{\rho} \frac{d\rho}{dr} + \frac{P}{T} \frac{dT}{dr} \quad (76)$$

Assume that the mean molecular weight  $\mu$  is constant:

$$\frac{dP}{dr} = \frac{P}{\rho} \frac{d\rho}{dr} + \frac{P}{T} \frac{dT}{dr} \quad (77)$$

Now, use the adiabatic relation between pressure and volume:

$$PV^\gamma = \text{const} \quad (78)$$

Or, in terms of density  $\rho$  (since  $V = \frac{1}{\rho}$ ):

$$P = K\rho^\gamma \quad (79)$$

where  $\gamma = \frac{C_P}{C_V}$  is the adiabatic index and  $K$  is a constant. Taking the derivative:

$$\frac{dP}{dr} = \gamma \frac{P}{\rho} \frac{d\rho}{dr} \quad (80)$$

Substitute in Eq. 77:

$$\gamma \frac{P}{\rho} \frac{d\rho}{dr} = \frac{P}{\rho} \frac{d\rho}{dr} + \frac{P}{T} \frac{dT}{dr} \quad (81)$$

Subtracting terms:

$$(\gamma - 1) \frac{P}{\rho} \frac{d\rho}{dr} = \frac{P}{T} \frac{dT}{dr} \quad (82)$$

Solving for  $\frac{dT}{dr}$ :

$$\frac{dT}{dr} = (\gamma - 1) \frac{T}{\rho} \frac{d\rho}{dr} \quad (83)$$

Or, using the pressure gradient directly:

$$\left. \frac{dT}{dr} \right|_{\text{ad}} = \left( 1 - \frac{1}{\gamma} \right) \frac{T}{P} \frac{dP}{dr} \quad (84)$$

This is the adiabatic temperature gradient, denoted  $\nabla_{\text{ad}}$ , and describes how the temperature of a rising convective element changes with radius under adiabatic conditions.

5) *Convective Stability: The Schwarzschild Criterion:* To determine whether a stellar layer is stable against convection, we compared the actual temperature derivative in the star to the adiabatic temperature derivative. The relevant criterion is the **Schwarzschild stability criterion**:

$$\left| \frac{dT}{dr} \right|_{\text{rad}} > \left| \frac{dT}{dr} \right|_{\text{ad}}, \quad (85)$$

Hence, the actual temperature decreases with radius faster than the temperature of an adiabatically rising fluid element. In this case, the displaced element remains warmer (and less dense) than its surroundings and continues to rise, initiating sustained convective motion.

When this condition is satisfied, convection occurs because radiative transport is insufficient, typically in regions of high opacity or strong energy flux, requiring a steep temperature gradient to carry energy outward. If the radiative temperature gradient exceeds the adiabatic threshold, the stratification becomes unstable, and the motions of the bulk fluid (convection) become the dominant energy transport mechanism.

Conversely, if

$$\left| \frac{dT}{dr} \right|_{\text{rad}} < \left| \frac{dT}{dr} \right|_{\text{ad}}, \quad (86)$$

convection does not occur because the displaced fluid element becomes cooler (and denser) than its surroundings and returns to its original position, maintaining convective stability.

This quantitative criterion is fundamental in stellar modeling. For example, low-mass stars like the Sun exhibit convective outer layers, while massive stars typically have convective cores due to their high luminosities and opacities.

Figure 7 clearly illustrates the energy transport zones within a star, linking the processes of radiative diffusion and convection to the star's mass. Radiative transport, governed by the radiative gradient equation, is efficient in regions where opacity is low, such as the Sun's core. However, convective transport becomes dominant in areas where the temperature gradient exceeds the adiabatic gradient, leading to thermal instability and the movement of gas masses. As shown in the image, low-mass stars exhibit convection in the outer layers, while more massive stars have a convective core. The juxtaposition of these zones demonstrates how the two mechanisms work together to maintain the thermal and structural balance of the star.

#### E. Stellar Radiation Laws: Stefan-Boltzmann and Wien's Law

The energy produced in the core of a star by nuclear fusion must be transported to its surface and eventually radiated into space. This outward radiation is governed by the physics of black-body emission, which provides a powerful framework for understanding stellar luminosity, temperature, radius, and color. Two of the most fundamental relations in this context are the Stefan-Boltzmann and Wien's law.

The Stefan-Boltzmann law states that the total energy radiated per unit time (luminosity) by a blackbody is proportional

to the fourth power of its effective temperature and to the surface area. Since a star approximates a blackbody, its luminosity  $L$  can be expressed as:

$$L = 4\pi R^2 \sigma T_{\text{eff}}^4 \quad (87)$$

where  $R$  is the radius of the star,  $T_{\text{eff}}$  is the effective surface temperature, and  $\sigma \approx 5.67 \times 10^{-8} \text{ W} \cdot \text{m}^{-2} \cdot \text{K}^{-4}$  is the Stefan-Boltzmann constant. This equation reveals that more luminous stars can be either larger or hotter. Importantly, since the temperature is raised to the fourth power, even modest increases in temperature result in large increases in luminosity. For example, doubling the surface temperature results in an increase in luminosity by a factor of sixteen. This explains why hot, blue stars are typically much more luminous than cooler red stars of similar size.

While the Stefan-Boltzmann law quantifies the amount of energy a star emits, Wien's displacement law determines the spectral location of that emission. It links the temperature of a blackbody with the wavelength at which it emits the most strongly, given by:

$$\lambda_{\text{max}} = \frac{b}{T} \quad (88)$$

where  $\lambda_{\text{max}}$  is the peak emission wavelength,  $T$  is the surface temperature, and  $b \approx 2.90 \times 10^{-3} \text{ m} \cdot \text{K}$  is Wien's constant. According to this relation, hotter stars emit more strongly at shorter wavelengths, placing their peak emission in the ultraviolet or blue part of the spectrum. Cooler stars, in contrast, peak at longer wavelengths such as red or even infrared. As a result, the color of a star directly reflects its surface temperature. For example, the blue-white star Rigel has a temperature of about 12,000 K, while the red supergiant Betelgeuse is much cooler, at approximately 3,500 K.

These principles are well illustrated in "Fig. 7", which shows blackbody curves for temperatures of 4000 K, 5777 K (close to the Sun's temperature), and 7000 K. As the temperature increases, the emission peak shifts towards shorter wavelengths, in accordance with Wien's law, and the total

## Heat Transfer of Stars

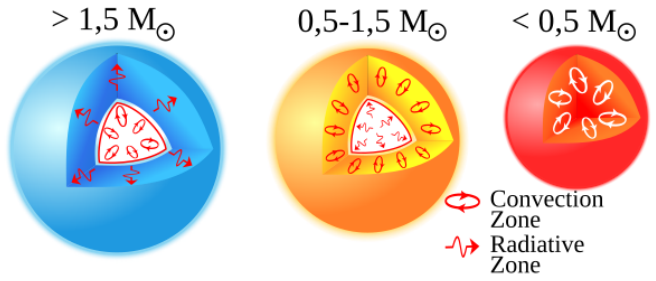


Fig. 7. Internal structure of stars of different masses, highlighting radiative zones and convective zones. Energy is transported by radiation in the core and by convection in the outer layers in stars similar to the Sun. In more massive stars, the opposite occurs: convection dominates in the core while radiation carries energy through the outer layers.

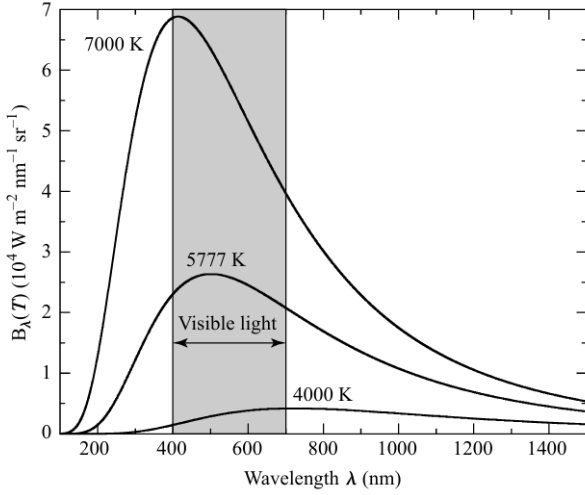


Fig. 8. Blackbody radiation curves for three stellar temperatures: 4000 K, 5777 K, and 7000 K. The shaded region represents the range of visible light. As temperature increases, the peak of the spectral radiance  $B_\lambda(T)$  shifts to shorter wavelengths (Wien's law), and the total area under each curve—proportional to the luminosity  $L$ —grows rapidly (Stefan-Boltzmann law). Thus, the integral of  $B_\lambda(T)$  over all wavelengths directly determines the total energy output  $L$ , showing how hotter stars are not only brighter, but also emit more of their energy at shorter wavelengths.

emitted energy increases rapidly, as predicted by the Stefan-Boltzmann law. The shaded area represents the visible spectrum, highlighting how hotter stars emit more in the blue and UV spectrum, while cooler stars radiate mostly in the red and infrared.

Together, these two radiation laws allow astronomers to infer critical stellar properties. By observing a star's color or spectrum, its temperature can be estimated; combining this with its luminosity enables the calculation of the radius. Tracking changes in these quantities over time also reveals how a star evolves. These principles are foundational in astrophysics and are directly used in constructing the Hertzsprung-Russell diagram, which classifies stars according to their luminosity and temperature, revealing patterns tied to different stages of stellar evolution.

#### F. Spectral Classification of Stars

The spectral classification of stars is a cornerstone of stellar astrophysics, providing essential information about a star's temperature, luminosity, and atmospheric composition. This system, originally developed by early twentieth-century astronomers such as Annie Jump Cannon, organizes stars based on the absorption features present in their spectra, which are themselves determined primarily by surface temperature.

The stars are categorized into spectral types using the sequence: **O – B – A – F – G – K – M**, ordered from the hottest to the coolest. **O-type** stars exhibit temperatures above 30,000 K and appear blue in color, while **M-type** stars are the coolest, with surface temperatures below 3,700 K, and appear red. Our Sun, for instance, is a G2 V star, with a surface temperature of about 5,800 K.

Each spectral type is further subdivided into 10 subclasses (from 0 to 9), allowing for finer granularity (e.g., B0 to B9, where B0 is hotter than B9). Furthermore, stars are also classified by luminosity class, ranging from I (supergiants) to V (main-sequence stars such as the Sun). A full stellar classification therefore includes both spectral and luminosity information; for example, the Sun's classification, G2 V, indicates a main-sequence star of spectral type G.

These spectral classes are not only useful for temperature estimation, but also reveal details about a star's chemical composition and physical state. For instance, strong hydrogen Balmer lines are most prominent in A-type stars, while cooler K- and M-type stars show molecular bands, such as titanium oxide (TiO), that are not present in hotter stars.

The table below (Table I) summarizes the main characteristics of each spectral class, including their typical colors, surface temperature ranges, and well-known stellar examples.

Understanding spectral classification is essential for interpreting the Hertzsprung-Russell diagram (previously discussed), since the horizontal axis of the H–R diagram is effectively a representation of spectral type and temperature. When plotted alongside luminosity, stars fall into distinct groupings that correlate with their evolutionary stages.

This classification system thus forms the observational foundation upon which stellar structure and evolution models are built.

#### G. Stellar Lifetime as a Function of Mass

Stars evolve through well-defined stages during their lifetimes, and the time they spend in each phase, especially on the main sequence, is deeply tied to their mass. From previous chapters, we have seen how stars in the main sequence are categorized by spectral type, color, and temperature. Here, we turn to the quantitative relationship between a star's mass and its luminosity, and how this relationship influences stellar longevity.

*1) Mass-Luminosity Relation:* The mass-luminosity relation describes how the luminosity  $L$  of a star in the main sequence depends on its mass  $M$ . Empirically, this relation is often approximated by a power law:

$$L \propto M^\alpha \quad (89)$$

For most main-sequence stars, the exponent  $\alpha$  is approximately 3.5, though it varies slightly across the mass range. This means that a star twice as massive as the Sun can be over ten times more luminous. The steepness of this relation has profound consequences for how long stars live.

As shown in "Fig. 9", stars of spectral types O and B (with masses over  $10M_\odot$ ) have extremely high luminosities and short lifespans, on the order of millions of years. In contrast, low-mass M-type stars, with less than  $0.5M_\odot$ , shine faintly but burn their fuel slowly, allowing them to remain in the main sequence for trillions of years.

TABLE I  
SPECTRAL CLASSIFICATION OF STARS BY TEMPERATURE, COLOR, AND EXAMPLE STARS

Spectral Class	Color	Temperature Range (K)	Example Stars
O	Blue	30,000 – 60,000	
B	Blue-white	10,000 – 30,000	$\zeta$ Puppis, HD 93129A
A	White	7,500 – 10,000	Rigel, Spica
F	Yellow-white	6,000 – 7,500	Sirius, Vega
G	Yellow	5,000 – 6,000	Procyon, Canopus
K	Orange	3,500 – 5,000	Sun (G2 V), Alpha Centauri A
M	Red	2,000 – 3,500	Arcturus, Aldebaran
			Betelgeuse, Proxima Centauri

2) *Estimating Stellar Lifetimes:* To estimate a star's main-sequence lifetime, we consider the ratio of the fuel available (which scales with mass) to the rate at which it is consumed (luminosity):

$$t_{\text{MS}} \propto \frac{M}{L} \propto \frac{M}{M^\alpha} = M^{1-\alpha} \quad (90)$$

Using  $\alpha \approx 3.5$ , we find:

$$t_{\text{MS}} \propto M^{-2.5} \quad (91)$$

This inverse relation shows that stellar lifetimes decrease dramatically with increasing mass. For example:

- A star with  $M = 2M_\odot$  lives about 0.18 times longer than the Sun.
- A red dwarf with  $M = 0.3M_\odot$  may live more than 100 times longer than the Sun.

This dramatic difference underscores how stellar mass is the dominant factor in determining a star's lifespan. Although massive stars live fast and die young, low-mass stars are long-lived cosmic embers, still burning long after high-mass stars have ended in spectacular supernovae.

#### *Astrophysical Implications and Connection to the H-R Diagram*

This mass-dependent lifetime has major implications for both galactic evolution and stellar demographics. Most of the bright, massive stars we observe today—such as O and B types—are relatively young because their high luminosities result in rapid fuel consumption and short main-sequence lifetimes. In contrast, the numerous, faint M dwarfs, despite their abundance, consume their hydrogen fuel so slowly that they remain on the main sequence for trillions of years and have not yet had time to evolve significantly since the universe's formation.

Understanding this mass-luminosity-lifetime relation is essential to interpret the Hertzsprung–Russell (H-R) diagram, which maps stellar luminosity versus temperature or spectral class. In stellar clusters, the location of the upper main-sequence turnoff provides a powerful age indicator: clusters with turnoff points at higher luminosities contain younger stars, while those where only low-mass stars remain on the main sequence are much older.

By combining this relation with the spectral classification system, we gain a deeper understanding of the evolutionary state of stars. High-mass O and B stars lie at the upper left

of the H-R diagram and evolve rapidly into supergiants or explode as supernovae, leaving behind neutron stars or black holes. Lower-mass K and M stars, residing in the lower right, evolve very slowly and can remain stable for tens to hundreds of billions of years.

This interconnected framework, linking stellar mass, luminosity, temperature, spectral type, and lifetime, forms the cornerstone of modern stellar astrophysics. It allows astronomers to decode stellar populations, trace galactic history, and model stellar evolution across cosmic time.

#### IV. DEATH OF THE STARS

The final stages of a star's life are primarily determined by its initial mass. Once a star exhausts the nuclear fuel in its core, it follows a distinct evolutionary path based on this mass. The gravitational equilibrium that has maintained the star throughout most of its life becomes unsustainable, leading to dramatic and often violent outcomes. This chapter delves into the various types of stellar remnants and the physical mechanisms responsible for their formation.

The concluding phases of stellar evolution represent some of the most dynamic and insightful processes in astrophysics. Although earlier chapters have explored the physical principles governing stellar structure and evolution, such as the main sequence phase and the fundamental equations of stellar equilibrium, this section focuses specifically on how stars meet their end and what remains once nuclear fusion ceases in their cores.

The initial mass of a star on the zero age main sequence (ZAMS) is the primary factor determining its evolutionary path and final fate. This mass not only dictates the temperature and pressure conditions necessary for nuclear fusion but also determines how and when the star will exhaust its nuclear fuel, undergo gravitational collapse, and form a compact remnant.

As shown in Figure "Fig. 10", stellar evolution diverges significantly based on the initial mass: low-mass stars evolve into white dwarfs, while high-mass stars end in supernova explosions, forming neutron stars or black holes.

During the main sequence, stars maintain hydrostatic equilibrium via thermal pressure from nuclear fusion. Once core fusion ceases, this equilibrium collapses. Gravity overtakes any residual thermal pressure, triggering collapse, the outcome of which depends on whether quantum degeneracy pressure (from electrons or neutrons) can resist further compression.

Three broad outcomes arise, based on stellar mass:

- Stars with  $M \lesssim 8 M_{\odot}$ : Eject outer envelopes as planetary nebulae, leaving behind carbon–oxygen white dwarfs supported by electron degeneracy pressure.
- Stars with  $8 M_{\odot} \lesssim M \lesssim 20 M_{\odot}$ : Undergo core-collapse supernovae, resulting in neutron stars supported by neutron degeneracy pressure.
- Stars with  $M \gtrsim 20$ – $25 M_{\odot}$ : Collapse into black holes when even degeneracy pressure fails, leading to event-horizon formation as described by general relativity.

These boundaries are not absolute. The outcome is influenced by metallicity, rotation, mass-loss rates, and binary interactions. For instance, a white dwarf in a binary system that accretes enough mass to exceed the Chandrasekhar limit ( $\sim 1.4 M_{\odot}$ ) may undergo a Type Ia supernova rather than remain stable.

In the following sections, we will examine the physics behind each evolutionary endpoint: from the fading remnants of white dwarfs to the ultra-dense interiors of neutron stars and the extreme curvature of spacetime around black holes. This analysis integrates theoretical models with observational data, including pulsars, supernova remnants, and black hole imaging, highlighting the complexity and significance of stellar death and the compact objects it leaves behind.

#### A. Low-Mass Stars ( $M < 8 M_{\odot}$ ): White dwarfs

White dwarfs represent the final evolutionary stage of low- and intermediate-mass stars (with initial masses up to approximately  $8$ – $10 M_{\odot}$ ). These stellar remnants are extremely dense and compact. Unlike main-sequence stars, where thermal pressure balances gravity, white dwarfs are supported by *electron degeneracy pressure*, a quantum mechanical effect that prevents further collapse.

**1) The Condition for Degeneracy:** At any temperature above absolute zero, some of the quantum states with energy less than the Fermi energy  $\varepsilon_F$  will become vacant,

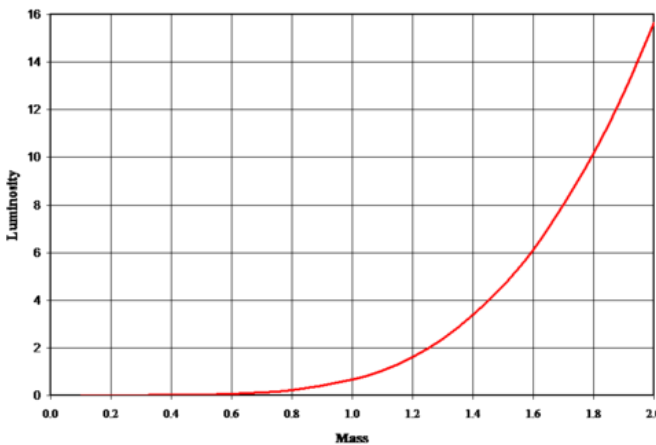


Fig. 9. Plot of luminosity  $L$  as a function of stellar mass  $M$ . The main sequence stars lie along a well-defined curve, indicating that more massive stars are vastly more luminous. This steep increase in luminosity with mass explains the rapid fuel consumption and shorter lifetimes of massive stars.

as electrons gain thermal energy and occupy higher-energy states. Although complete degeneracy no longer holds exactly when  $T > 0$  K, the assumption of complete degeneracy remains an excellent approximation under the extremely high densities found in the interiors of white dwarfs. Assuming full ionization, the number of electrons per unit volume is given by:

$$n_e = \left( \frac{Z}{A} \right) \frac{\rho}{m_H}, \quad (92)$$

where  $Z$  is the number of protons per nucleus,  $A$  is the total number of nucleons (protons + neutrons) per nucleus,  $\rho$  is the mass density of the white dwarf,  $m_H$  is the mass of a hydrogen atom.

In a degenerate electron gas at zero temperature, the electrons fill all available quantum states up to Fermi energy  $E_F$ . This configuration gives rise to a pressure known as *electron degeneracy pressure*, which plays a central role in supporting white dwarfs against gravitational collapse.

The number of available quantum states per unit energy (density of states) for a non-relativistic free electron gas in three dimensions is given by:

$$g(E) = \frac{V}{2\pi^2} \left( \frac{2m}{\hbar^2} \right)^{3/2} \sqrt{E} \quad (93)$$

where  $V$  is the volume,  $m_e$  is the electron mass.

Integrating up to the Fermi energy  $E_F$ , the total number of electrons  $N$  is:

$$\begin{aligned} N &= \int_0^{E_F} g(E) dE \\ &= \frac{V}{2\pi^2} \left( \frac{2m}{\hbar^2} \right)^{3/2} \int_0^{E_F} E^{1/2} dE \\ &= \frac{V}{3\pi^2} \left( \frac{2m}{\hbar^2} \right)^{3/2} E_F^{3/2} \end{aligned} \quad (94)$$

The total energy  $E$  of the degenerate gas is:

$$\begin{aligned} E &= \int_0^{E_F} E \cdot g(E) dE \\ &= \frac{V}{2\pi^2} \left( \frac{2m}{\hbar^2} \right)^{3/2} \int_0^{E_F} E^{3/2} dE \\ &= \frac{V}{5\pi^2} \left( \frac{2m}{\hbar^2} \right)^{3/2} E_F^{5/2} \end{aligned} \quad (95)$$

Using the Eq. 94 and 95, we can write the total energy  $E$  of the electron gas is related to the Fermi energy by:

$$E = \frac{3}{5} N E_F \quad (96)$$

The Fermi energy  $E_F$  for a completely degenerate, non-relativistic electron gas is given by:

$$E_F = \frac{\hbar^2}{2m} (3\pi^2 n_e)^{2/3}, \quad (97)$$

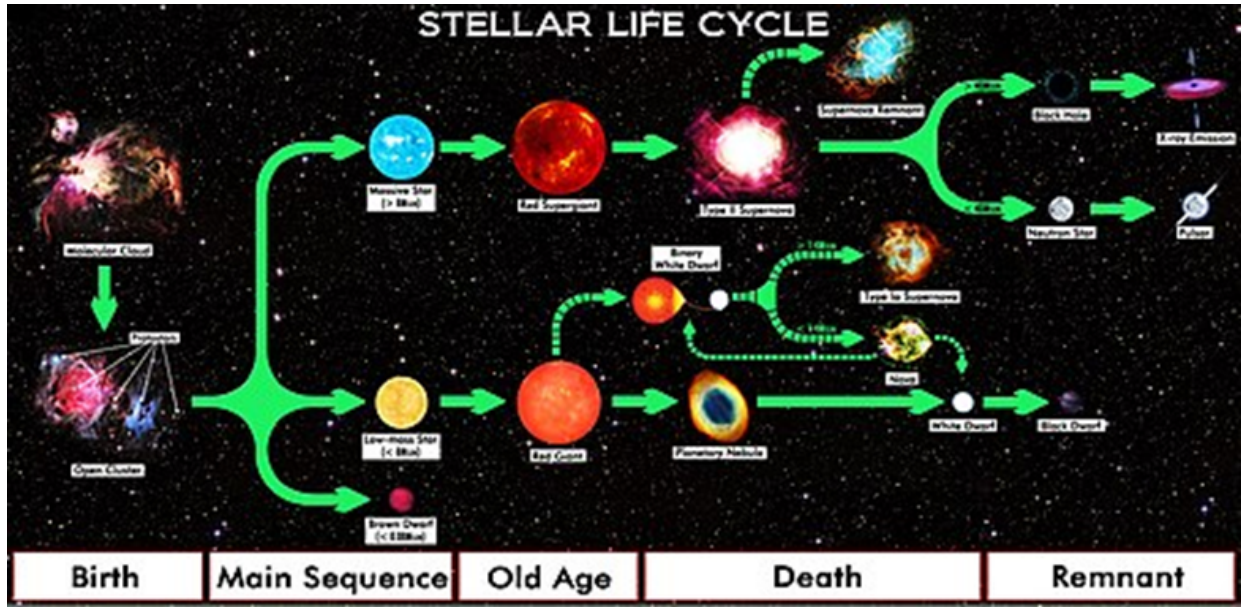


Fig. 10. Stellar Life Cycle. Diagram illustrating the evolutionary paths of stars based on their initial mass. All stars originate from molecular clouds and begin as protostars. Low-mass stars ( $M < 8 M_{\odot}$ ) evolve into red giants and end their lives as white dwarfs, often preceded by the formation of planetary nebulae. In binary systems, white dwarfs may undergo novae or Type Ia supernovae. Massive stars ( $M > 8 M_{\odot}$ ) evolve into red supergiants and undergo core-collapse supernovae (Type II), forming neutron stars or black holes, depending on the remnant core mass. Final stellar remnants are sustained by quantum degeneracy pressure (in the case of white dwarfs and neutron stars) or result in space-time singularities (black holes). The diagram follows the star's lifecycle in stages: formation, main sequence, late evolution, death, and remnant.

Substituting  $N = n_e V$  and using Eqs. 96 and 97 we obtain the following:

$$E = \frac{3}{5} N \frac{\hbar^2}{2m} \left( \frac{3\pi^2 N}{V} \right)^{2/3} \quad (98)$$

From thermodynamics, the pressure is defined by:

$$P = - \left( \frac{\partial E}{\partial V} \right)_N \quad (99)$$

Now, using Eqs. 98 and 99, we obtain the following:

$$P = \frac{2}{5} n E_F = \frac{2}{3} \frac{E}{V} \quad (100)$$

Substituting Eq. 98 into Eq. 100 and using  $N = n_e V$ , we obtain the pressure of a completely degenerate, non-relativistic electron gas at  $T = 0$  is:

$$P = \frac{\hbar^2}{m_e} \frac{(3\pi^2)^{2/3}}{5} n_e^{5/3} \quad (101)$$

Furthermore, by using Eq. 92, we have:

$$P = \frac{\hbar^2}{m_e} \frac{(3\pi^2)^{2/3}}{5} \left( \left( \frac{Z}{A} \right) \frac{\rho}{m_H} \right)^{5/3} \quad (102)$$

This degeneracy pressure exists even in the absence of thermal motion, arising purely from the Pauli exclusion principle. It is what counterbalances gravitational collapse in white dwarfs until relativistic effects become significant. However, a more accurate description requires numerical modeling that accounts for more complex physics, including partial degeneracy, finite (non-zero) temperatures, and variations in chemical composition.

2) **The Chandrasekhar Limit:** The requirement that the electron degeneracy pressure must support a white dwarf star has profound implications. In 1931, the Indian physicist Subrahmanyan Chandrasekhar announced his discovery that there is a maximum mass for white dwarfs.

Starting from the condition of hydrostatic equilibrium, Eq. 38, using the (unrealistic) assumption of constant density,  $M_r = \frac{4}{3}\pi r^3 \rho$ , we have the following:

$$\frac{dP}{dr} = - \frac{G \cdot \frac{4}{3}\pi r^3 \rho \cdot \rho}{r^2} = - \frac{4}{3}\pi G \rho^2 r. \quad (103)$$

This is easily integrated using the boundary condition that  $P(R) = 0$  on the surface to obtain the pressure as a function of  $r$ ,

$$P(r) = \frac{2}{3}\pi G \rho^2 (R^2 - r^2). \quad (104)$$

The relation between the radius  $R_{\text{wd}}$  of a white dwarf and its mass  $M_{\text{wd}}$  can be found by setting the estimate of the central pressure Eq. 104 equal to the electron degeneracy pressure Eq. 102:

$$\frac{2}{3}\pi G \rho^2 R_{\text{wd}}^2 = \frac{(3\pi^2)^{2/3}}{5} \frac{\hbar^2}{m_e} \left( \frac{Z}{A} \frac{\rho}{m_H} \right)^{5/3}. \quad (105)$$

Using the density expression  $\rho = \frac{M_{\text{wd}}}{\frac{4}{3}\pi R_{\text{wd}}^3}$  (assuming constant density), we obtain an estimate for the radius of the white dwarf:

$$R_{\text{wd}} \approx \frac{(18\pi)^{2/3}}{10} \frac{\hbar^2}{Gm_e M_{\text{wd}}^{1/3}} \left( \frac{Z}{A m_H} \right)^{5/3}. \quad (106)$$

Thus, the equation reveals a surprising implication: the mass of the white dwarf and its radius are related in such a way that  $M_{\text{wd}} R_{\text{wd}}^3 = \text{constant}$ .

*3) Relativistic Degeneracy and the Chandrasekhar Limit:* As we have just shown, the equilibrium of a white dwarf star in the non-relativistic regime is sustained by the degeneracy pressure of electrons. In that case, the pressure satisfies a polytropic equation of state of the form  $P = K\rho^{5/3}$ , and the resulting mass-radius relation yields the surprising implication that the product  $M_{\text{wd}} R_{\text{wd}}^3$  remains constant. However, this relation begins to break down as the central density increases to the point where the electrons become relativistic.

In the relativistic regime, the momentum of the electrons can no longer be approximated by  $p = mv$ , and instead must be treated using special relativity. As the Fermi momentum of the electron increases, the corresponding energy approaches the linear relation  $E \approx pc$ , characteristic of ultra-relativistic particles.

This approximation becomes valid in the high-density limit of white dwarfs, where the electron degeneracy pressure increases as the electrons are forced into higher momentum states because of the Pauli exclusion principle. At sufficiently high densities, the Fermi energy greatly exceeds the rest mass energy of the electron ( $E_F \gg m_e c^2$ ), placing the system in the ultra-relativistic regime. Therefore, the use of the approximation  $E \approx pc$  is justified when deriving the Chandrasekhar mass limit, as it captures the asymptotic behavior of the electron gas in the densest stable white dwarfs.

To derive the expression for the pressure of a degenerate Fermi gas at zero temperature, we begin with the classical concept of pressure as the result of momentum transfer due to particle collisions with the walls of a container. Consider a large number of non-interacting particles confined in a cubic box of volume  $V = A\Delta x$ , where  $A$  is the cross-sectional area and  $\Delta x$  is the length along the  $x$  direction. Each particle undergoes perfectly elastic collisions with the walls and is characterized by its momentum  $\vec{p}$  and velocity  $\vec{v}$ .

Let us analyze the force exerted by a single particle on the wall perpendicular to the  $x$ -axis. For each collision, the momentum change imparted to the wall is  $\Delta p_x = 2p_x$  due to the reversal of the  $x$  component of the momentum. The time interval between successive collisions with the same wall by this particle is  $\Delta t = 2\Delta x/v_x$ , since the particle must travel to the opposite wall and back. The average force exerted by the particle on the wall is then given by Newton's second law as

$$f = \frac{\Delta p_x}{\Delta t} = \frac{2p_x}{2\Delta x/v_x} = \frac{p_x v_x}{\Delta x}. \quad (107)$$

Since pressure is defined as force per unit area and the volume is  $V = A\Delta x$ , we write the pressure contribution from one particle as:

$$P = \frac{f}{A} = \frac{p_x v_x}{A\Delta x} = \frac{p_x v_x}{V}. \quad (108)$$

To obtain the total pressure from all particles, we must consider the distribution of particles over momenta. In a gas of fermions at temperature  $T = 0$ , the momentum states are occupied up to the Fermi momentum  $p_F$ , and unoccupied beyond. The number of states per unit volume with momenta between  $p$  and  $p + dp$  is given by the density of states in the momentum space for spin-1/2 particles:

$$g(p) dp = \frac{p^2}{\pi^2 \hbar^3} dp. \quad (109)$$

The total pressure is obtained by integrating over all the momentum states, accounting for the fact that the particles have random directions. On average, due to isotropy, the  $x$  component of the momentum squared is one-third of the total:

$$\langle p_x v_x \rangle = \frac{1}{3} p v. \quad (110)$$

Therefore, the pressure is given by:

$$P = \frac{1}{3} \int_0^{p_F} p v(p) g(p) dp. \quad (111)$$

This expression provides a general framework for computing the pressure of a degenerate Fermi gas at zero temperature, applicable to both non-relativistic and relativistic regimes, depending on the functional form of the group velocity  $v(p) = \frac{dp}{dE}$ . In the ultra-relativistic limit, where the energy-momentum relation is approximated by  $E(p) \approx pc$ , the group velocity becomes  $v(p) = c$ . Under these conditions, the integral can be explicitly evaluated and the resulting expression of the pressure takes the form  $P \propto \rho^{4/3}$ , where  $\rho$  is the mass density of the degenerate electron gas.

To derive the explicit form of the degeneracy pressure in the ultra-relativistic regime, we begin with the general expression for the pressure of a zero-temperature Fermi gas Eq. (111), along with the constant group velocity  $v(p) = c$  valid in the ultra-relativistic limit and the density of states for spin- $\frac{1}{2}$  fermions Eq. (109), and the pressure integral becomes:

$$P = \frac{c}{3\pi^2 \hbar^3} \int_0^{p_F} p^3 dp. \quad (112)$$

Evaluating the integral, we find that the pressure becomes as flowing:

$$P = \frac{c}{12\pi^2 \hbar^3} p_F^4. \quad (113)$$

Next, we relate the Fermi momentum  $p_F$  to the number density of electrons  $n_e$ . For a completely degenerate gas of electrons:

$$n_e = \frac{1}{3\pi^2 \hbar^3} p_F^3, \quad (114)$$

which gives:

$$p_F = (3\pi^2 \hbar^3 n_e)^{1/3}. \quad (115)$$

Substituting this into the pressure expression, Eq. (113):

$$P = \frac{c}{12\pi^2\hbar^3} (3\pi^2\hbar^3 n_e)^{4/3} = \frac{(3\pi^2)^{1/3}}{4} \hbar c n_e^{4/3}. \quad (116)$$

Since the density of the number of electrons is related to the mass density by Eq. (92), the pressure becomes:

$$P = K' \rho^{4/3}, \quad (117)$$

with:

$$K' = \frac{(3\pi^2)^{1/3}}{4} \hbar c \left( \left( \frac{Z}{A} \right) \frac{1}{m_H} \right)^{4/3}. \quad (118)$$

The pressure-density relation  $P \propto \rho^{4/3}$  corresponds to the critical case of gravitational stability, beyond which no stable equilibrium configuration exists. In this regime, the total mass of the white dwarf becomes independent of its radius. To determine the corresponding limiting mass, we equate the central pressure of the hydrostatic equilibrium, Eq. (104), with the relativistic degeneracy pressure in Eq. (117). Using the density expression  $\rho = \frac{M_{\text{Ch}}}{\frac{4}{3}\pi R^3}$ , this leads to:

$$M_{\text{Ch}} = \sqrt{\frac{6}{\pi}} \left( \frac{K'}{G} \right)^{3/2}. \quad (119)$$

Substituting Eq. (118) into Eq. (119), we find:

$$M_{\text{Ch}} \sim \frac{3\sqrt{2\pi}}{8} \left( \frac{\hbar c}{G} \right)^{3/2} \left( \left( \frac{Z}{A} \right) \frac{1}{m_H} \right)^2. \quad (120)$$

This result is remarkable in that it depends only on fundamental physical constants: Planck's constant  $\hbar$ , the speed of light  $c$ , and Newton's gravitational constant  $G$ , as well as the compositional parameters  $Z/A$  and the proton mass  $m_H$ . For a typical carbon–oxygen white dwarf, where  $Z/A = 0.5$ , the simplified derivation yields the following:

$$M_{\text{Ch}} \approx 0.44 M_{\odot}. \quad (121)$$

However, this estimate is based on a uniform density approximation. A more accurate treatment, which accounts for the full variation of pressure and density throughout the star using a relativistic polytropic model, gives a corrected value:

$$M_{\text{Ch}} \approx 1.44 M_{\odot}. \quad (122)$$

which is the well-known Chandrasekhar limit.

4) *Precise Determination of the Chandrasekhar Mass via the Lane-Emden Equation:* The simplified derivation of the Chandrasekhar limit assumes a constant density and yields an approximate maximum mass. To obtain a more accurate result, one must solve the full equations of stellar structure using a relativistic polytropic equation of state. This leads to the Lane-Emden equation, which describes the internal structure of a spherically symmetric polytropic star in hydrostatic equilibrium.

Starting from the equations of stellar structure introduced earlier, namely the hydrostatic equilibrium condition Eq. (38)

and the mass continuity equation Eq. (30), we now assume a polytropic relation of the form:

$$P = K \rho^{1+\frac{1}{n}}, \quad (123)$$

with  $n$  the polytropic index and  $K$  a constant determined by the physics of the equation of state, in this case the relativistic electron degeneracy pressure. For this regime,  $K$  corresponds to the constant  $K'$  defined previously in Eq. (118).

To simplify the system, we introduce dimensionless variables through the substitutions:

$$r = a\xi, \quad \rho(r) = \rho_c \theta^n(\xi), \quad (124)$$

where  $\rho_c$  is the central density and  $\theta(\xi)$  is a dimensionless function representing the normalized density profile.

The parameter  $a$  sets the radial scaling and is defined to eliminate constants in the resulting equations:

$$a^2 = \frac{(n+1)K}{4\pi G} \rho_c^{(1/n)-1}, \quad (125)$$

so that the system becomes independent of the choice of central density and can be expressed in universal, scale-free form.

Substituting into Eq. (31), we obtain the mass enclosed within radius  $r = a\xi$ ,

$$M(r) = 4\pi a^3 \rho_c \int_0^\xi \xi'^2 \theta^n(\xi') d\xi' \equiv 4\pi a^3 \rho_c m(\xi), \quad (126)$$

with

$$m(\xi) = \int_0^\xi \xi'^2 \theta^n(\xi') d\xi'. \quad (127)$$

Differentiating Eq. (127) with respect to  $\xi$ , we obtain its differential form:

$$\frac{dm}{d\xi} = \xi^2 \theta^n(\xi). \quad (128)$$

The pressure becomes  $P = K \rho_c^{1+1/n} \theta^{n+1}$ , and its derivative is

$$\frac{dP}{dr} = \frac{1}{a} \frac{dP}{d\xi} = \frac{1}{a} K \rho_c^{1+\frac{1}{n}} (n+1) \theta^n \frac{d\theta}{d\xi}. \quad (129)$$

The right-hand side of Eq. (38) becomes

$$\begin{aligned} -\frac{GM(r)\rho(r)}{r^2} &= -\frac{G \cdot 4\pi a^3 \rho_c m(\xi) \cdot \rho_c \theta^n}{a^2 \xi^2} \\ &= -4\pi G a \rho_c^2 \frac{m(\xi)}{\xi^2} \theta^n. \end{aligned} \quad (130)$$

Equating both sides of the hydrostatic equilibrium equation, Eq. (38), using the pressure gradient derived from the polytropic equation of state from Eq. (129), and the gravitational term expressed with the mass profile from Eq. (130), and canceling the common factor  $\theta^n$ , we find:

$$K \rho_c^{1+\frac{1}{n}} (n+1) \frac{d\theta}{d\xi} = -4\pi G a^2 \rho_c^2 \frac{m(\xi)}{\xi^2}. \quad (131)$$

Substituting the expression for  $a^2$  from Eq. (125), we see that the constants cancel:

$$(n+1) K \rho_c^{1+\frac{1}{n}} = 4\pi G a^2 \rho_c^2, \quad (132)$$

so we are left with the simplified equation,

$$\frac{d\theta}{d\xi} = -\frac{m(\xi)}{\xi^2}. \quad (133)$$

Differentiating both sides with respect to  $\xi$ , and using Eq. (128), we obtain the Lane-Emden equation:

$$\frac{1}{\xi^2} \frac{d}{d\xi} \left( \xi^2 \frac{d\theta}{d\xi} \right) = -\theta^n. \quad (134)$$

For white dwarfs in the ultra-relativistic regime, the equation of state becomes  $P = K' \rho^{4/3}$ , as derived in Eq. (117). Comparing this with the general polytropic form  $P = K \rho^{1+\frac{1}{n}}$  in Eq. (123), we identify the polytropic index as  $n = 3$ .

Substituting  $n = 3$  into the Lane-Emden equation, Eq. (134), we obtain a second-order nonlinear ordinary differential equation for the dimensionless function  $\theta(\xi)$ , with boundary conditions:

$$\theta(0) = 1, \quad \frac{d\theta}{d\xi}(0) = 0.$$

This equation does not admit an analytic solution for  $n = 3$ , so it must be solved numerically. The first zero of  $\theta(\xi)$ , denoted  $\xi_1$ , corresponds to the radius of the white dwarf (in dimensionless units), and the dimensionless mass is calculated by means of the following equation:

$$\omega_3 \equiv m(\xi_1) = -\xi_1^2 \frac{d\theta}{d\xi} \Big|_{\xi=\xi_1}. \quad (135)$$

The numerical integration yields the following:

$$\xi_1 \approx 6.89685, \quad \omega_3 \approx 2.02069. \quad (136)$$

The total physical mass of the white dwarf is given by:

$$M = 4\pi a^3 \rho_c \omega_3, \quad (137)$$

which follows directly from the integral of the mass in dimensionless form, Eq. (126), and the definition of the dimensionless mass function  $m(\xi)$  in Eq. (135), evaluated at  $\xi = \xi_1$  as  $\omega_3 = m(\xi_1)$ .

For  $n = 3$ , the scale factor  $a$  defined in Eq. (125) becomes:

$$a^2 = \frac{K'}{\pi G} \rho_c^{-2/3} \Rightarrow a^3 \rho_c = \left( \frac{K'}{\pi G} \right)^{3/2}. \quad (138)$$

Substituting into the mass expression, Eq. (137) the Chandrasekhar mass becomes:

$$M_{\text{Ch}} = 4\pi \omega_3 \left( \frac{K'}{\pi G} \right)^{3/2}, \quad (139)$$

using  $K'$  from Eq. (118) and the value of  $\omega_3$  from Eq. (136) with  $Z/A = 0.5$ , we find:

$$M_{\text{Ch}} \approx 1.44 M_{\odot}. \quad (140)$$

This is the precise Chandrasekhar limit: the maximum mass that a white dwarf can support against gravitational collapse via relativistic electron degeneracy pressure alone. Beyond this limit, the electron degeneracy pressure is no longer sufficient to balance the star's self-gravity.

Figure 11 shows the mass-radius relation for white dwarfs at  $T = 0$  K. Notably, no white dwarf with a mass exceeding the Chandrasekhar limit has ever been observed. The existence of this limit sets a fundamental boundary in stellar evolution. If the core of a dying star exceeds this critical mass, it becomes dynamically unstable and undergoes gravitational collapse. The white dwarf phase ends abruptly, giving rise to a core-collapse supernova. The stellar envelope is expelled in a violent explosion, while the core contracts further into a neutron star or, if massive enough, a black hole.

### B. Core-Collapse Supernovae and Their Observational Signatures

Core-collapse supernovae are among the most energetic events in stellar evolution. They mark the terminal stage in the lives of massive stars, those with initial main-sequence masses typically exceeding  $8 M_{\odot}$  [5]. When these stars exhaust their nuclear fuel, they can no longer resist gravitational contraction. The result is a catastrophic collapse of the core and a dramatic explosion that disseminates newly forged elements into the interstellar medium [4].

*Collapse Mechanism and Core Dynamics:* In the late stages of stellar evolution, massive stars develop an iron core through successive fusion of lighter elements. Since iron fusion is endothermic, it does not contribute to supporting the star against gravity [8]. Once the core mass exceeds the Chandrasekhar limit (approximately  $1.4 M_{\odot}$ ), the electron degeneracy pressure fails, initiating rapid gravitational collapse [5].

Within milliseconds, the density of the core reaches nuclear values ( $\sim 3 \times 10^{17} \text{ kg m}^{-3}$ ). At this point, the collapse is temporarily halted by neutron degeneracy pressure, producing a rebound known as a core bounce. This bounce generates an outward propagating shock wave. However, the shock quickly stalls because of photodisintegration of heavy nuclei and intense neutrino emission [6].

The currently accepted mechanism for reviving the stalled shock is the delayed neutrino heating model. Neutrinos, re-

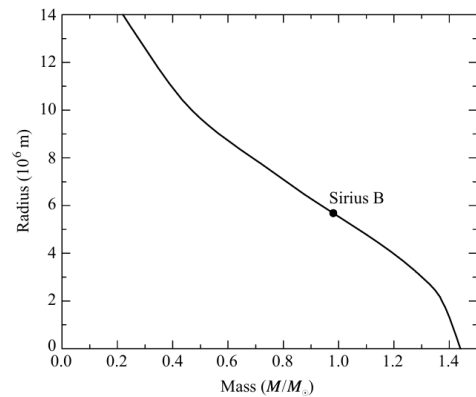


Fig. 11. Mass-radius relation for white dwarfs at  $T = 0$  K. The curve shows that as the mass increases, the radius decreases due to increased gravitational compression. The location of Sirius B is marked. No white dwarf exceeds the Chandrasekhar limit of approximately  $1.44 M_{\odot}$ .

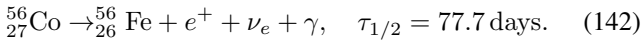
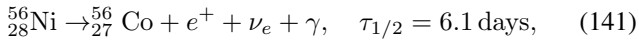
leased in vast quantities from the proto-neutron star, deposit a fraction of their energy in the region just behind the shock, re-energizing it and triggering the explosion of the outer layers [7].

*Remnant Formation: Neutron Stars and Black Holes:* The nature of the compact remnant formed depends on the progenitor's mass and metallicity. If the stellar core is less massive than about  $2.5 M_{\odot}$ , the neutron degeneracy pressure can support it, resulting in the formation of a neutron star, a dense object composed almost entirely of neutrons.

For more massive cores, the collapse continues beyond neutron degeneracy support, forming a black hole. Metal-rich stars can lose substantial mass through stellar winds, allowing stars with initial masses even higher than  $25 M_{\odot}$  to leave behind neutron stars [5]. In both cases, the gravitational collapse releases a total energy of  $E_{\text{binding}} \sim 3 \times 10^{46} \text{ J}$ , most of which is carried away by neutrinos, approximately  $10^{58}$  of them, escaping over a few seconds. This neutrino luminosity briefly outshines the combined output of all stars in the observable universe.

*Light Curves and Radioactive Decay:* The light curve of core-collapse supernovae provides critical information about the explosion mechanism and post-explosion physics. A classic example is the Type II-P supernova, which exhibits a plateau phase that lasts 80 to 100 days. This plateau arises due to hydrogen recombination in the extended stellar envelope, which maintains a roughly constant photospheric temperature of  $\sim 5000 \text{ K}$  [5].

A substantial portion of the late-time luminosity is powered by radioactive decay of unstable isotopes synthesized in the explosion. The decay chain begins with  $^{56}\text{Ni}$ :



These gamma rays thermalize in the ejecta, sustaining the observed brightness [5]. The evolution of the number of nuclei is governed by the decay law:

$$N(t) = N_0 e^{-\lambda t}, \quad \lambda = \frac{\ln 2}{\tau_{1/2}}. \quad (143)$$

This leads to a linear decline in the bolometric magnitude:

$$\frac{dM_{\text{bol}}}{dt} = 1.086 \lambda, \quad (144)$$

where  $M_{\text{bol}}$  is the bolometric magnitude and  $\lambda$  is the decay constant [5]. This relationship allows identification of the isotopes present by comparing the observed slope with theoretical expectations. Long-lived isotopes such as  $^{57}\text{Co}$  (271 days),  $^{22}\text{Na}$  (2.6 years) and  $^{44}\text{Ti}$  (47 years) contribute to the late-time light curve and nebular emission.

*Observational Breakthrough: SN 1987A:* The explosion of SN 1987A in the Large Magellanic Cloud provided an unprecedented opportunity to study a nearby core-collapse event in detail. The progenitor was a blue supergiant (Sk

$-69^{\circ}202$ ), and the explosion deviated from the typical Type II-P behavior [5].

Figure 12 illustrates the bolometric light curve of SN 1987A, highlighting the contributions of radioactive isotopes such as  $^{56}\text{Ni}$ ,  $^{56}\text{Co}$ , and  $^{57}\text{Co}$ . The light curve slowly reached a peak in  $\sim 80$  days, reaching an absolute bolometric magnitude of only  $-15.5$ . Approximately  $0.075 M_{\odot}$  of  $^{56}\text{Ni}$  was synthesized, with gamma-ray lines at 847 and 1238 keV confirming the presence of  $^{56}\text{Co}$  [5]. The late-time luminosity showed contributions from  $^{57}\text{Co}$  and  $^{44}\text{Ti}$ , consistent with the model predictions.

Doppler broadening of the gamma-ray lines indicated expansion velocities of thousands of km/s, and neutrinos from the collapse were directly detected by the Kamiokande and IMB detectors, confirming theoretical expectations.

*Supernova Remnants and Circumstellar Structures:* The aftermath of core-collapse supernovae includes extended structures known as supernova remnants. These remnants are composed of shocked stellar ejecta and swept-up interstellar material, often emitting at radio, optical, and X-ray wavelengths.

The remnant of SN 1987A is particularly complex, featuring a bright inner ring (diameter  $\sim 0.42$  pc) and two outer rings aligned in a bipolar configuration. These structures likely originate from mass loss episodes of the progenitor during its red supergiant and blue supergiant phases. The Hubble Space Telescope has captured the interaction of the shock front with the inner ring since 1996, leading to clumpy bright regions where the shock excites dense material [5].

#### C. Neutron Stars – The Remnants of Intermediate-Mass Stars

After the supernova explosion that marks the death of an intermediate-mass star, the remaining core, if below the maximum mass limit, undergoes a dramatic transformation into a neutron star. These objects, only about 10 km in radius but containing up to twice the mass of the Sun, represent the densest form of matter outside black holes. Their properties

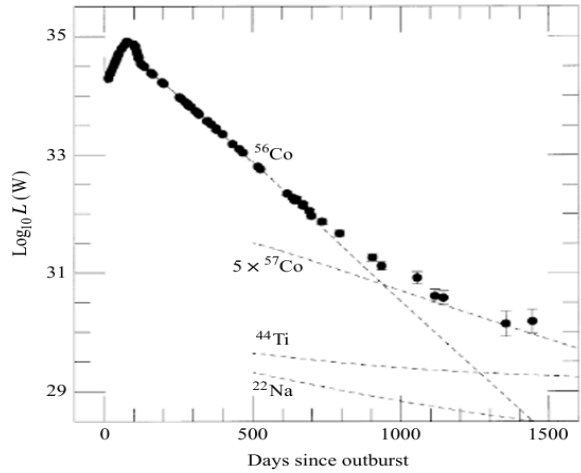


Fig. 12. Bolometric light curve of SN 1987A, highlighting decay contributions from  $^{56}\text{Ni}$ ,  $^{56}\text{Co}$ , and  $^{57}\text{Co}$ .

arise directly from fundamental conservation laws and from the physics of matter under extreme conditions.

*1) The Equation of State:* The equation of state (EOS) describes how pressure relates to the density inside neutron stars, where matter exists under extreme conditions. At lower densities, nucleons are bound in nuclei, balanced by nuclear attraction and Coulomb repulsion. As density rises, electrons become relativistic and induce neutronization: electrons capture protons to form neutrons, increasing neutron-rich nuclei. Upon reaching approximately  $4 \times 10^{14} \text{ kg/m}^3$ , free neutrons drip out of the nuclei, forming a superfluid neutron component alongside nuclei and electrons. At densities above nuclear saturation, nuclei dissolve into a uniform fluid of neutrons, protons, and electrons, with neutrons forming a superfluid and protons a superconducting phase. The EOS at these densities remains uncertain due to complex nuclear interactions and possible exotic matter, which critically affects neutron star structure and stability.

*2) The Chandrasekhar Limit for Neutron Stars and Neutron Star Models:* A neutron star can be approximately modeled as a self-gravitating Fermi gas of degenerate neutrons. The density of neutrons can be estimated as  $n_n = \rho/m_n$ , where  $m_n$  is the neutron mass. By applying an approach similar to the one used in the derivation of Eq. 106 for white dwarfs, we obtain the following mass-radius scaling relation:

$$R_{ns} \approx \left( \frac{18\pi^2}{10} \right)^{2/3} \frac{\hbar^2}{GM_{ns}^{1/3}} \left( \frac{1}{m_n} \right)^{8/3}. \quad (145)$$

A typical result from more detailed models yields the inverse relation:

$$M_{ns}R_{ns}^3 = \text{constant}, \quad (146)$$

indicating that more massive neutron stars are generally more compact.

The maximum mass for a non-rotating neutron star is estimated to be about  $2.2 M_\odot$ , increasing to approximately  $2.9 M_\odot$  for rapidly rotating stars.

Figure 13 illustrates the internal structure of a  $1.4 M_\odot$  neutron star. The star structure can be divided into three main regions: the outer crust, composed of heavy nuclei and degenerate electrons; the inner crust, where free neutrons coexist with increasingly neutron-rich nuclei; and the core, which contains superfluid neutrons, superconducting protons, and possibly exotic phases consisting of pions or other sub-nuclear particles. The precise composition of the core remains uncertain and is a central topic in modern nuclear astrophysics.

*Rapid Rotation and Conservation of Angular Momentum:* A key prediction about neutron stars, confirmed observationally in pulsars, is their rapid rotation. This arises naturally from the conservation of angular momentum during the collapse of the progenitor star's iron core. Assuming here for simplicity to lose no mass during collapse, so  $M_{\text{core}} = M_{\text{wd}} = M_{\text{ns}}$ , and

modeling the core as a sphere with moment of inertia of the form  $I = CMR^2$ , angular momentum conservation gives

$$I_i \omega_i = I_f \omega_f \Rightarrow \omega_f = \omega_i \left( \frac{R_i}{R_f} \right)^2. \quad (147)$$

In terms of the rotation period  $P$ , we obtain

$$P_f = P_i \left( \frac{R_f}{R_i} \right)^2. \quad (148)$$

Using Eqs. 106 and 145, and assuming the neutron mass is nearly equal to the mass of the hydrogen atom, the collapse from a core radius typical of a white dwarf to that of a neutron star yields a ratio is:

$$\frac{R_i}{R_f} \approx \frac{m_n}{m_e} \left( \frac{Z}{A} \right)^{5/3} = 512. \quad (149)$$

where  $Z/A = 26/56$  for iron has been used.

Thus, a progenitor with  $P_{\text{core}} = 1350$  s (as observed in white dwarf 40 Eridani B) results in a neutron star with a rotation period of

$$P_{ns} \approx 3.8 \times 10^{-6} P_{\text{core}} \approx 5 \times 10^{-3} \text{ s}. \quad (150)$$

This prediction matches the millisecond periods observed in young pulsars.

*Thermal Evolution and Neutrino Cooling:* Newly formed neutron stars are extremely hot, with  $T \sim 10^{11}$  K. In the first day, they cool primarily through *neutrino emission*, particularly via the URCA process:

$$n \rightarrow p^+ + e^- + \bar{\nu}_e, \quad (151)$$

$$p^+ + e^- \rightarrow n + \nu_e. \quad (152)$$

This cooling is efficient until the nucleons degenerate, when the core temperature drops to  $\sim 10^9$  K. After this, other neutrino processes dominate for about 1000 years. Later, photon emission from the surface governs the cooling. At a

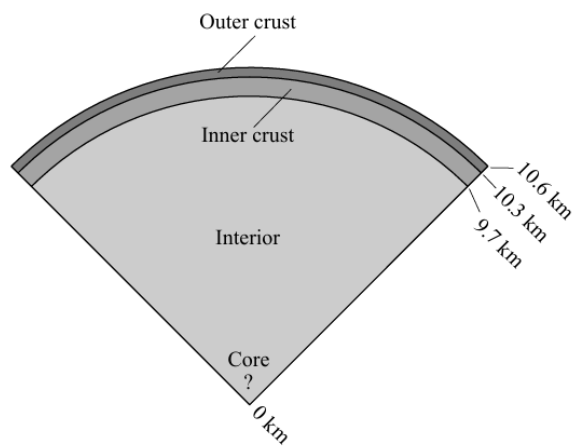


Fig. 13. A structural model of a  $1.4 M_\odot$  neutron star. The crust (outer and inner) extends from  $\sim 9.7$  to  $10.6$  km, overlying the dense core and interior.

few hundred years old, the internal temperature is around  $10^8$  K and the surface stabilizes near  $10^6$  K.

Using the Stefan-Boltzmann law,

$$L = 4\pi R^2 \sigma T^4, \quad (153)$$

for a neutron star with  $R \approx 10^4$  m and  $T \approx 10^6$  K, the thermal luminosity is

$$L \approx 7.13 \times 10^{25} \text{ W}, \quad (154)$$

comparable to the Sun, though radiated mainly in X-rays. According to Wien's law,

$$\lambda_{\max} = \frac{(500 \text{ nm})(5800 \text{ K})}{T} \approx 2.9 \text{ nm}, \quad (155)$$

this radiation falls in the X-ray regime, consistent with observations from ROSAT, ASCA, and Chandra.

Having examined the structure, composition, and evolution of neutron stars, stellar remnants supported against gravitational collapse by neutron degeneracy pressure, we now turn to one of their most remarkable observable manifestations, the pulsars.

**Pulsars:** are highly magnetized, rapidly rotating neutron stars that emit regular pulses of electromagnetic radiation, typically detected in the radio band. They were discovered in 1967 by Jocelyn Bell and her advisor Anthony Hewish while studying the scintillation of quasars. Bell noticed remarkably regular signals, initially dubbed "LGM" (Little Green Men) due to their extraordinary precision.

Pulsars share several key features:

- **Rotation periods:** range from 0.0014 s (Terzan 5ad) to 11.8 s (PSR 1841-0456), with an average of about 0.795 s.
- **Extreme precision:** Their periods are incredibly stable and can be measured with greater accuracy than the best atomic clocks. For example, PSR 1937+214 has a period known to more than 15 decimal places.
- **Period increase:** all pulsars gradually slow down over time. The rate of change is given by  $\dot{P} = dP/dt$ , usually on the order of  $10^{-15}$ .
- **Characteristic lifetime:** defined as  $P/\dot{P}$ , usually around  $10^7$  years, although it can reach several hundred million years.

**Physical Models:** Several mechanisms were considered to explain the pulsar signals.

- 1) **Binary systems:** ruled out due to incompatibility with the observed period increases and the expected energy loss via gravitational waves.
- 2) **Pulsating stars:** is ruled out because the known oscillation modes of neutron stars and white dwarfs do not match the observed pulsar periods.
- 3) **Rotating stars:** this is the accepted model. A rotating neutron star with a magnetic axis misaligned with its rotational axis emits radiation beams. When the beam crosses Earth's line of sight, we detect a pulse.

This behavior is commonly referred to as the "lighthouse effect," illustrated in Figure 14, where the misalignment between

the magnetic and rotation axes causes the emission beam to sweep across space like a cosmic beacon.

Rapid rotation of neutron stars is explained by the conservation of angular momentum during stellar collapse. The minimum rotation period is constrained by the balance between gravity and centrifugal force at the equator:

$$\omega_{\max}^2 R = \frac{GM}{R^2} \Rightarrow P_{\min} = 2\pi \sqrt{\frac{R^3}{GM}}, \quad (156)$$

where  $P_{\min} = 2\pi/\omega_{\max}$ ,  $R$  is the radius and  $M$  the mass of the star. For a typical neutron star ( $M = 1.4M_{\odot}$ ,  $R \approx 10$  km), we find  $P_{\min} \approx 0.5$  ms, which agrees with the fastest pulsars observed.

#### D. High-Mass Stars: Black holes

When the most massive stars in the universe, those with initial masses exceeding about 20 to 25 times that of the Sun, reach the end of their nuclear lifetimes, gravity wins its final battle. No known force can stop the collapse of their cores, leading to the formation of one of the most extreme objects in the cosmos: a black hole. These regions of spacetime possess gravitational fields so intense that not even light can escape beyond their event horizon. In this section, we delve into the physics that governs their formation, examine their fundamental properties, and consider the observational signatures that reveal their hidden presence in the universe.

1) **Schwarzschild Radius and Newtonian Prelude:** As early as 1783, the English natural philosopher John Michell speculated that a sufficiently massive and compact star might exert such strong gravitational attraction that even light could not escape its surface. Using Newtonian gravity and assuming light behaves as a stream of particles, one can estimate the critical radius at which this occurs by setting the escape velocity equal to the speed of light:

$$v_{\text{esc}} = \sqrt{\frac{2GM}{R}}, \quad (157)$$

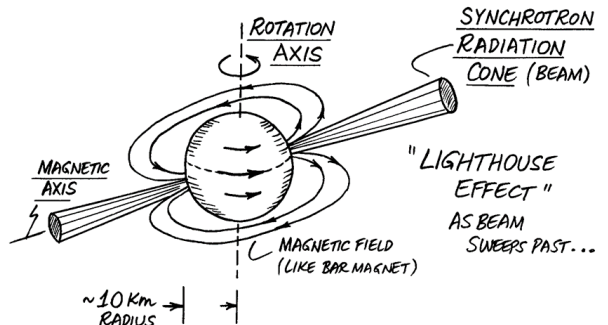


Fig. 14. Illustration of the lighthouse model for pulsars. The misalignment between the magnetic axis and the rotation axis causes the synchrotron radiation beam to sweep across space. When this beam crosses Earth's line of sight, we detect a pulse.

Solving for  $R$  when  $v_{\text{esc}}$  is equal to the speed of light  $c$  gives the classical form of the Schwarzschild radius:

$$R_S = \frac{2GM}{c^2}, \quad (158)$$

where  $R_S$  defines the radius within which light cannot escape. In solar mass units, this becomes:

$$R_S \approx 2.95 \frac{M}{M_\odot} \text{ km}. \quad (159)$$

Although derived from Newtonian principles, this result remarkably anticipates the event horizon in general relativity, formalized over a century later by Karl Schwarzschild.

2) *Schwarzschild Metric and Event Horizon:* In 1916, Karl Schwarzschild derived the exact solution to Einstein's field equations for a nonrotating, uncharged mass. The Schwarzschild line element is

$$ds^2 = \left( cdt \sqrt{1 - \frac{2GM}{rc^2}} \right)^2 - \left( \frac{dr}{\sqrt{1 - \frac{2GM}{rc^2}}} \right)^2 - r^2 d\Omega^2, \quad (160)$$

where  $d\Omega^2 = d\theta^2 + \sin^2 \theta d\phi^2$  [5]. This metric reveals significant effects of gravity on spacetime, particularly near the Schwarzschild radius, Eq.158.

The surface  $r = R_S$  defines the *event horizon*, a limit beyond which no information can escape back to a distant observer. Marks the point where gravity becomes so strong that even light cannot escape. A schematic representation of a black hole and its event horizon is shown in Fig. 15.

At  $r = R_S$ , the square roots in the metric vanish and the spacetime geometry exhibits extreme behavior. The proper time  $d\tau$  measured by a clock at this radius becomes zero, indicating that the time appears to come to a halt from the perspective of a distant observer. This phenomenon is not due to the failure of the laws of physics, but reflects the deep warping of spacetime near the horizon.

To investigate how light behaves near this boundary, we consider a radial photon trajectory ( $d\theta = d\phi = 0$ ) and set  $ds = 0$ . Using the Schwarzschild metric, we find:

$$\left( cdt \sqrt{1 - \frac{2GM}{rc^2}} \right)^2 = \left( \frac{dr}{\sqrt{1 - \frac{2GM}{rc^2}}} \right)^2. \quad (161)$$

Solving for the coordinate speed of light,  $dr/dt$ , we obtain:

$$\frac{dr}{dt} = c \left( 1 - \frac{2GM}{rc^2} \right) = c \left( 1 - \frac{R_S}{r} \right). \quad (162)$$

Far from the mass ( $r \gg R_S$ ), the coordinate speed of light approaches  $c$ , consistent with a flat spacetime. However, as  $r \rightarrow R_S$ , the coordinate speed of light  $dr/dt \rightarrow 0$ . From the point of view of a distant observer, light appears to be "frozen" at the event horizon.

3) *A Trip into the Black Hole:* An object as bizarre as a black hole deserves closer scrutiny. Imagine investigating it by sending a radio pulse toward the event horizon from a safe distance and observing its reflection. How long will it take for a radio photon (or any photon) to reach the event horizon from a radial coordinate  $r \gg R_S$  and then return?

Integrating Eq. (162) to compute the round-trip time for a photon between two arbitrary values of  $r_2$  and  $r_1$ , (assuming that  $r_2 > r_1$ ) yields

$$\Delta t = \frac{r_2 - r_1}{c} + \frac{R_S}{c} \ln \left( \frac{r_2 - R_S}{r_1 - R_S} \right). \quad (163)$$

This expression shows that as  $r_1 \rightarrow R_S$ , the time  $\Delta t \rightarrow \infty$ . Thus, from the perspective of a distant observer, light, or any signal, never actually reaches the horizon in finite coordinate time. This leads to the appearance *frozen star*: objects appear to freeze on the event horizon, never fully vanishing from view.

Consequently, any object crossing  $R_S$  becomes undetectable to external observers. The event horizon acts as a one-way boundary, beyond which no information or matter can escape. A star collapsing within its Schwarzschild radius forms a **black hole**, not marked by a physical surface, but by a mathematical boundary in spacetime.

4) *Mass Ranges of Black Holes:* Black holes are observed across a wide range of masses:

- **Stellar-mass black holes** ( $3-15 M_\odot$ ): Formed from the core-collapse of massive stars during supernovae. These are the most common type of black holes detected through X-ray binaries and gravitational wave observations.
- **Intermediate-mass black holes (IMBHs)** ( $10^2-10^4 M_\odot$ ): These are hypothesized to exist in globular clusters or dwarf galaxies, inferred from ultraluminous X-ray sources. Their origin remains uncertain and is an active area of research.
- **Supermassive black holes (SMBHs)** ( $10^5-10^9 M_\odot$ ): Found at the centers of most galaxies, including the Milky Way. The black hole at the Galactic center, Sagittarius A\* (Sgr A\*), has a mass of approximately  $3.7 \times 10^6 M_\odot$ .

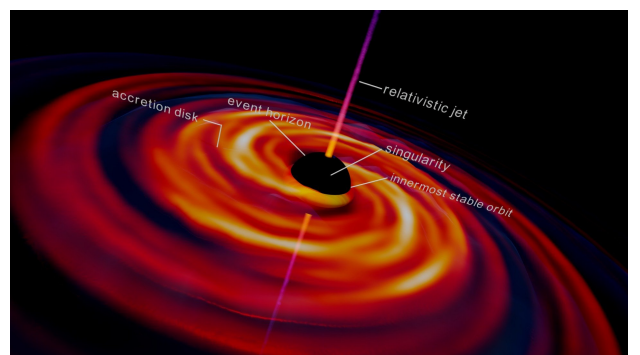


Fig. 15. Schematic illustration of the Schwarzschild black hole with event horizon at  $r = R_S$ .

- **Primordial black holes:** Hypothetical black holes formed in the early universe due to density fluctuations. Their masses could range from subatomic scales ( $< 1 \text{ kg}$ ) up to  $10^5 M_{\odot}$ .

5) *The No-Hair Theorem:* No matter how black holes form, general relativity tells us that they are completely characterized by only three observable quantities: mass  $M$ , angular momentum  $J$ , and electric charge  $Q$ . This result is known as the **No-Hair Theorem**.

During gravitational collapse, any complex features of matter are radiated away, primarily through gravitational waves. Once the event horizon forms, the external spacetime settles into a stationary state described by one of the classical black hole solutions: Schwarzschild (non-rotating, uncharged), Kerr (rotating), Reissner–Nordström (charged), or Kerr–Newman (rotating and charged). Black holes do not have other attributes or adornments, a condition commonly expressed by saying that “a black hole has no hair”.

There is a maximum angular momentum a black hole can possess, given by:

$$J_{\max} = \frac{GM^2}{c} \quad (164)$$

Beyond this limit, the event horizon would disappear, exposing a *naked singularity*, which is forbidden by the **Law of Cosmic Censorship**.

6) *Rotating Black Holes and Frame Dragging:* Realistic black holes are expected to rotate because of the angular momentum inherited from their progenitor stars. The spacetime geometry around a rotating (Kerr) black hole differs significantly from the non-rotating Schwarzschild solution. In particular, rotation introduces the following key features:

- **An oblate event horizon:** The event horizon is flattened along the axis of rotation as a consequence of the spin of the black hole.
- **A ring singularity:** Instead of a point singularity, rotation stretches the central singularity into a ring-shaped structure.
- **An ergosphere:** A region outside the event horizon where spacetime itself is dragged in the direction of the black hole’s rotation, making it impossible for any object to remain stationary relative to distant observers.

This dragging of spacetime is known as the **frame dragging**, or the Lense–Thirring effect. Inside the ergosphere, objects are compelled to co-rotate with the black hole due to the intense twisting of spacetime. The outer boundary of the ergosphere is called the **static limit**.

Although frame dragging around Earth is extremely weak, it has been experimentally confirmed by the Gravity Probe B mission launched by Stanford University in 2004 [9]. However, near a rotating black hole, this effect is dramatically amplified and must be incorporated into any accurate physical description of black hole environments.

*Observational Signatures:* Although black holes emit no light, they can be observed through their interactions with surrounding matter and via gravitational waves:

- **X-ray binaries:** Matter from a companion star accretes onto the black hole, forming a hot accretion disk. The intense gravitational energy release causes strong X-ray emission.
- **Stellar dynamics:** Motions of stars orbiting around invisible central masses (e.g., near Sgr A\*) reveal the presence of a supermassive black hole.
- **Gravitational waves:** The inspiral and merger of two black holes generate ripples in spacetime. These have been detected by the LIGO and Virgo collaborations since 2015.

These signatures provide robust, indirect evidence of black holes, confirming the predictions of general relativity and helping constrain the mass and spin distributions of the black hole population.

## V. SCIENTIFIC REFLECTIONS: THE ROLE OF MATHEMATICAL MODELING

In this work, I have explored how theoretical astrophysics transforms the fundamental laws of gravity, thermodynamics, and nuclear physics into predictive models of stellar behavior. From the formation of stars in collapsing gas clouds to their final fates as white dwarfs, neutron stars, or black holes, stellar evolution is governed by complex relationships between pressure, temperature, density, and composition. Although the analysis presented here is primarily analytical—using scaling relations such as the mass–luminosity law and the lifetime–mass dependence, and interpreting results through the Hertzsprung–Russell diagram—the framework that supports these insights is inherently mathematical.

Rather than employing full-scale numerical simulations, I focused on simplified models that still capture the essential physical mechanisms behind stellar evolution. These models help explain why high-mass stars are more luminous and short-lived, and how a star’s initial mass determines whether it will end its life as a white dwarf, neutron star, or black hole. The analytical approach also reproduces key observational trends, offering intuitive understanding with minimal computational complexity.

The equations and concepts used here form the foundation for more advanced modeling tools used in professional astrophysics. That these simplified relations align well with observational data, ranging from stellar spectra and pulsar characteristics to star cluster populations, highlights the strength and relevance of the mathematical framework adopted.

Future extensions of this study could benefit from numerical modeling to refine predictions and explore effects not captured analytically, such as rotation, convection, or detailed time evolution. Nevertheless, even in its current form, this work demonstrates how mathematical reasoning provides deep insight into the life cycles of stars and remains a cornerstone of theoretical astrophysics.

## VI. CONCLUSION

This work has shown that mathematical modeling, anchored in conservation laws, stellar structure equations, and nuclear

physics, provides a deep, quantitative understanding of stellar lifecycles. From the rapid fuel consumption of O-type stars to the ultra-long lives of red dwarfs, and from the gentle cooling of white dwarfs to the violent births of neutron stars and black holes, our theoretical predictions align closely with astronomical data.

Looking ahead, key avenues for refining this picture include the following.

- Incorporating rotation and magnetic fields into analytic models (e.g., via perturbative expansions).
- Updating microphysical inputs: opacities and reaction rates based on laboratory and theoretical advances.
- Exploiting new observations (asteroseismology, gravitational-wave events) to test and calibrate theoretical relations.

By maintaining a close dialogue between simple analytic relations and ever-improving data, we can continue to sharpen the mathematical portrait of stars from birth to death.

#### REFERENCES

- [1] ESA/Webb Space Telescope. *Protostar L1527*. 2022. Image credit: ESA/Webb, NASA, CSA, and the MIRI instrument team. Available at: [https://www.esa.int/ESA\\_Multimedia/Images/2022/11/Protostar\\_L1527](https://www.esa.int/ESA_Multimedia/Images/2022/11/Protostar_L1527)
- [2] NASA/JPL, “Orion Nebula in Infrared,” *Spitzer Space Telescope*, 2006. <https://www.spitzer.caltech.edu/image/ssc2006-16a1-orion-in-the-infrared>
- [3] ESA/Hubble, “Hertzsprung–Russell Diagram,” <https://cdn.spacetelescope.org/archives/images/screen/heic0814hrdiagram.jpg>
- [4] I. Morison, *Introduction to Astronomy and Cosmology*, Wiley, 2008.
- [5] B. W. Carroll & D. A. Ostlie, *An Introduction to Modern Astrophysics*, 2nd ed., Pearson, 2017.
- [6] T. Padmanabhan, *Theoretical Astrophysics, Volume II: Stars and Stellar Systems*, Cambridge University Press, 2000.
- [7] M. Zeilik & S. A. Gregory, *Introductory Astronomy and Astrophysics*, 4th ed., Brooks Cole, 1997.
- [8] Kippenhahn, R., & Weigert, A. *Stellar Structure and Evolution*., Springer-Verlag, 1990.
- [9] Everitt, C. W. F., et al. (2011). “Gravity Probe B: Final Results of a Space Experiment to Test General Relativity.” *Physical Review Letters*, 106(22), 221101. <https://doi.org/10.1103/PhysRevLett.106.221101>